Defence Research and Development Canada
Recherche et développement pour la défense Canada

DEFENCE R&D DÉFENSE

Influence of solid target reflectivity and incident angle on depolarization ratio and reflected energy from polarized lights

Experimental results of the May 2008 field trial

Daniel A. Lavigne
DRDC Valcartier

Mélanie Breton
Aerex Avionique Inc.

Defence R&D Canada – Valcartier
Technical Report
DRDC Valcartier TR 2008-394
November 2009

Canada

Influence of solid target reflectivity and incident angle on depolarization ratio and reflected energy from polarized lights

Experimental results of the May 2008 field trial

Daniel A. Lavigne
DRDC Valcartier

Mélanie Breton
Aerex Avionique Inc.

Defence R&D Canada

Technical Report
DRDC Valcartier TR 2008-394
November 2009

Principal Author

Daniel A. Lavigne

Approved by

Jean-Marc Garneau
Section Head/SGE

Approved for release by

Christian Carrier
Chief Scientist

Abstract

Spectral sensors are commonly used to measure the intensity of optical radiation and to provide spectral information about the distribution of material components in a given scene, over a limited number of wave bands. By exploiting the polarization of light to measure information about the vector nature of the optical field across a scene, collected polarimetric images have the potential to provide additional information about the shape, shading, roughness, and surface features of targets of interest. The overall performance of target detection algorithms could thus be increased by exploiting these polarimetric signatures to discriminate man-made objects against different backgrounds.

In order to understand how the polarisation of light might help in the discrimination of solid targets from their background, a field trial was conducted at DRDC Valcartier between 14-16 May 2008. The approach consisted in evaluating the depolarization ratio of different solid targets using active polarization signatures at 532 nm. This technical report presents the set-up, the methodology and the type of targets measured during the trial. The targets used were segmented into eight groups: insulation, wood, metallic, environment, sand paper-type, industrial plastic-type, bottles and sand targets. Experimental results on the influence of solid target reflectivity and incident angle on depolarization ratio and reflected energy from polarized lights is also provided.

Résumé

Des capteurs spectraux, fonctionnant sur une plage spectrale limitée, sont couramment utilisés pour obtenir des informations sur la nature spectrale de certains matériaux présents dans une scène. En exploitant la polarisation de la lumière pour mesurer des informations sur le champ optique d'une scène, il est possible d'obtenir des images polarimetriques qui ont le potentiel d'accroître la connaissance sur la forme, la rugosité ainsi que les caractéristiques de surface de certaines cibles d'intérêt. La performance globale d'algorithmes de détection de cibles peut ainsi être accrue par l'exploitation de ces signatures polarimetriques pour discriminer des objets de l'arrière scène.

Pour comprendre comment la polarisation de la lumière peut aider à la discrimination de cibles solides, un essai a eu lieu à RDDC Valcartier entre le 14 et le 16 mai 2008. Cet essai consistait à évaluer le ratio de dépolarisation de certaines cibles solides par l'utilisation de leurs signatures polarimétriques actives à 532 nm. Ce rapport technique présente le montage expérimental, la méthodologie ainsi que les différentes cibles mesurées durant cet essai. Les cibles étaient divisées en huit groupes : les matériaux isolants, le bois, le métal, les cibles d'environnement, les papiers sablés, les plastiques industriels, les bouteilles et le sable. Des résultats expérimentaux sur l'influence de la réflectivité de ces cibles solides et l'angle d'incidence sur le ratio de dépolarisation et l'énergie réfléchie de la lumière polarisée sont également présentés.

Executive summary

Influence of solid target reflectivity and incident angle on depolarization ratio and reflected energy from polarized lights

Daniel A. Lavigne , Mélanie Breton ; DRDC Valcartier TR 2008-394; Defence R&D Canada; November 2009.

The objective of this research and development project is to discriminate solid targets using their respective active polarization signatures. Accordingly, reflectivities and depolarization ratios of solid targets were computed based on measurements using a dual images polarization lidar consisting of a Q switch laser operating at 532 nm, a telescope, and a gated intensified CCD camera from Andor Technology. Target measurements were collected at DRDC Valcartier in May 2008.

Numerous types of materials were employed as interesting targets, including: insulation, wood, metal, sand papers, composite plastic, concrete, grasses, wet and dry sands, and other environmental targets. Both linear and circular polarized lights were used in the field measurements, and four incident angles (0, 15, 30, and 45 degrees with respect to the vertical axis) were generated individually. It was shown that:

1. Metals (both bare and painted ones) are very special targets, showing very little depolarization at any incident angle. They were very reflective at angle 0 degree (with respect to the vertical axis), but their reflectivity dropped sharply when incident angle increases.

2. For most targets, the depolarization ratios generally increase when incident angle change from 0 to 30 degrees . However, when incident angle was further increased to 45 degrees, depolarization ratios decreased.

3. For most targets, high reflectivity usually corresponds to higher depolarization. But it is difficult to compare between targets from different category.

Beside the 532 nm lidar being used for the measurements, additional signatures were collected using a lidar operating at a wavelength of 1.57 μm. This was done in order to compare the differences in the polarimetric signatures of targets using two different collecting devices. Linear depolarization ratios of targets measured from lidar operating at 1.57 μm were usually higher than those acquired from lidar operating at 532 nm.

The polarimetric signatures collected from these solid targets will populate a reference library that will be used in future work involving the use of polarimetric signatures to discriminate solid targets against different backgrounds.

Sommaire

Influence of solid target reflectivity and incident angle on depolarization ratio and reflected energy from polarized lights

Daniel A. Lavigne , Mélanie Breton ; DRDC Valcartier TR 2008-394; R & D pour la défense Canada; novembre 2009.

L'objectif de ce projet de recherche est de discriminer des cibles d'intérêt en utilisant leurs signatures polarimétriques respectives. Ainsi, les ratios de réflectance et de dépolarisation de ces cibles ont été calculés en fonction des mesures utilisant un lidar imageur à double polarisation opérant à 532 nm et utilisant : un télescope, une caméra avec un intensificateur CCD de Andor Technology. Les mesures de ces cibles ont été recueillies à RDDC Valcartier au mois de mai 2008.

Plusieurs types de matériaux ont été employés comme cibles d'intérêt, incluant : isolants, bois, métaux, papiers sablés, plastiques, béton, gazon, sable humide et sec, et d'autres cibles environnementales. La lumière polarisée linéaire et circulaire a été utilisée et quatre angles incidents (0, 15, 30 et 45 degrés selon l'axe vertical) ont été générés individuellement. Is a été démontré que :

1. Les objects métalliques sont des cibles très spéciales, démontrant une faible dépolarisation indépendamment de l'angle incident. Ils sont très réflectifs à 0 $^{\circ}$ (selon l'axe vertical), mais leur réflectivité décroît abruptement lorsque l'angle incident augmente.

2. Pour des cibles, les ratios de dépolarisation augmentent généralement lorsque l'angle incident change de 0 à 30 degrés. Par contre, lorsque l'angle incident a augmenté à 45 degrés, les ratios de dépolarisation diminuent.

3. Pour la plupart des cibles, une haute réflectivité correspond habituellement à une forte dépolarisation. Cependant, il est difficile de comparer des cibles classées selon différentes catégories.

Juxtaposées aux mesures effectuées à l'aide du lidar 532 nm, des signatures additionnelles ont été acquises à des fins de comparaison en utilisant un lidar opérant à une longueur d'onde de 1.57 μm. Les ratios de dépolarisation linéaire des cibles mesurées à l'aide du lidar opérant à une longueur d'onde de 1.57 μm étaient généralement plus élevés que ceux générés par le lidar opérant à une longueur d'onde de 532 nm.

Les signatures polarimétriques acquises de cibles d'intérêts vont alimenter une librairie de référence. Celle-ci sera utilisée lors de travaux ultérieurs pour discriminer des cibles de leur arrière-plan, en utilisant leurs signatures polarimétriques respectives.

Acknowledgements

The authors would like to acknowledge the significant contribution of Gilles Roy, Sylvain Cantin, and Xiaoying Cao in the realisation of the field experiments conducted using DRDC Valcartier's compact aerosol dissemination chamber and the associated optical set-up and data analysis.

This page intentionally left blank.

Table of contents

List of figures

List of tables

1 Introduction

The Spectral and Geospatial Exploitation Section of Defence Research and Development Canada - Valcartier has the mandate to explore new surveillance sensor concepts to enhance the detection, recognition and identification of maritime, surface, and airborne targets. One of the Section's axes of research is to investigate new imaging technologies and concepts to improve the Canadian Forces surveillance and reconnaissance capabilities.

The use of electro-optical instruments and sensors in military operations has been increasing rapidly in recent years. The overwhelming advantages enjoyed by a force that owns devices like laser rangefinders, designators, night-vision goggles, day and night cameras and thermal imagers were evident during the last conflicts (90-91 Gulf war, Kosovo, Afghanistan, Iraq), when the U.S.-led various coalitions made extensive use of these technologies. During conflicts or peacekeeping missions in which the Canadian Forces have participated, the short-to-medium range capabilities of these optronic devices and their complementary role to radar were appreciated. Radars are well-known long-range, all-weather detection sensors, with generally poor resolution, as optronic sensors are shorter range, high-spatial resolution imaging devices. Today, almost all surveillance platforms are equipped with some electro-optical (EO) sensors, CCD cameras, and image intensified systems and thermal imaging sensors are among the most commonly used imaging devices. In the near future, it is expected that imaging systems using polarization could be added to the list.

Polarization is an important property of light and represents a fundamental concept in several technological fields such as imagery, telecommunication, medicine, and instrumentation. Many applications use active coherent illumination and analyze the variation of the polarization state of the optical signal [1, 2, 3, 4, 5]. Polarization of light has been used and studied by many people in the past for different applications [6, 7, 8, 9, 10, 11, 12].

This technical report investigates the target contrast enhancement obtained by analyzing the polarization of the reflected light from either a direct polarized laser source as encountered in active imagers or from natural ambient illumination [13, 14, 1, 2]. This technique is known as polarimetric imaging and is based on the discrimination property that man made objects will not depolarize light in the same manner than natural background will, thus implying their potential use for applications like target detection and target recognition. It has a strong potential for detecting objects that have a low contrast in classical intensity images. Furthermore, polarimetric imaging may also be used to discriminate some events of interest (e.g. tracks left in snow, disturb soil, etc.) against various types of natural background [5, 15, 16, 17, 18].

Accordingly, one of the objectives of the applied research project (ARP) entitled

Phenomenology and utility assessment study of the polarimetric EO imaging concept (15dk03) requires to deliver a complete study on the phenomenology and on the utility of the polarimetric EO imaging concept. Its main objective is to assess to what extent and under which illumination and environmental conditions the exploitation of polarimetric images is suitable to enable target detection and recognition for some events of interest. Previously, studies such as [19] and [20] in LWIR, [14] and [6] in the visible, have been made about the polarization properties in passive imaging of sample targets. Similarly, depolarization is used with lidar system to distinguish between liquid and solid phases of water in the atmosphere [21, 11]. However, there was no study showing the results between the degree of polarization in passive and the depolarization ratio in active systems.

Within the scope of this project, a field trial was carried out at DRDC Valcartier during 14-16 May 2008. The aim of this trial was to collect active polarization signatures of solid targets in order to discriminate them from their background. To do so, reflectivity and depolarization ratios of these solid targets have been measured with a dual image polarization lidar (consisting of a Q switch laser operating at 532 nm), a telescope and a gated intensified CCD camera from Andor Technology. Additionnaly, polarization signatures were collected using a lidar operating at a wavelength of 1.57 μm.

Different types of targets have been measured: construction materials and grass, textiles, woods, environmental targets, insulation materials, sands, composite plastics, and metals. The set-up was made of subtargets mounted onto a wooden board topped by a white and a black Spectralon. These experimental results will become a reference data for future work in imaging polarization.

Specifically, the objectives were:
- to gather information about the influence of different incident angles on the depolarization ratio of Spectralon;
- to gather information about the influence of different incident angles on the depolarization ratio and degree of polarization of selected targets;
- to build a polarization/depolarization signatures library to be a reference data for future work in imaging polarization.

This technical report is divided into 5 different sections. Section 2 presents the experimental set-up used to conduct the field trial, including the environmental chamber and the optical bed. The methodology used throughout this research project to calibrate the laser devices and to collect relevant polarimetric signatures is presented in section 3. Section 4 enumerates the different solid targets that were measured and presents the associated experimental findings. A summary of the experimental results is presented in section 5. Comparison wrt the depolarization ratios with the lidar operating at $1.57/mum$ is presented in section 6. Final conclusion and future

work are presented in section 7.

This work was performed under 15DK03 "Current and Emerging Image Exploitation Techniques" from May 2008 to May 2009.

This page intentionally left blank.

2 Experimental set-up

This section presents the experimental set-up used during the field trial. It includes the description of the environment chambers and the optical set-up used for collecting the polarization signatures of solid targets.

2.1 The environment chamber

The entire field trial took place in the north side of DRDC Valcartier, situated at the north side of Road 573. The targets were installed in the 22 meters long compact aerosol dissemination chamber (Figure 1), located in the experimental complex. Solid targets were installed at three-quarter end within the chamber, which could be established from 0 to 500 meters away from the electro-optic device. Figure 2 shows the experimental layout of the environmental chamber.

Figure 1: *The compact aerosol dissemination chamber*

Solid targets were set on an automated *Pan'n'Tilt* device where the angles were set precisely for each measurement. Targets were turned upside down at the end of an acquisition set since the laser beam was not wide enough to measure the targets panel as a whole. All measurements were collected during daytime. Figure 3 illustrates the environment chamber as viewed from the laboratory window and some targets installed on the *Pan'n'Tilt* device.

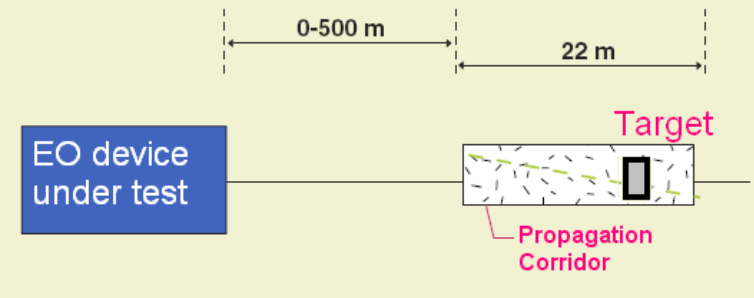

Figure 2: *Experimental layout*

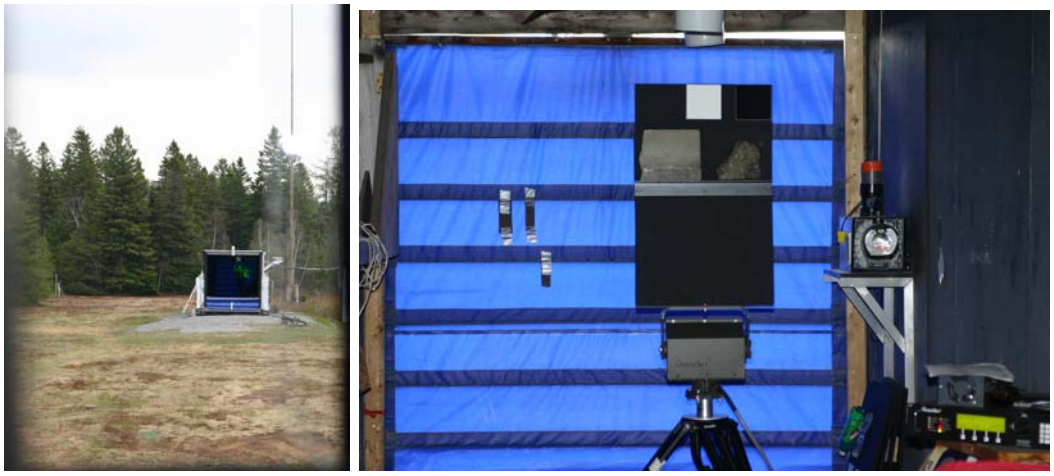

(a) Environment chamber (b) Targets and *Pan'n'Tilt*

Figure 3: *Environment chamber viewed from the laboratory window and example of targets installed on the Pan'n'Tilt*

2.2 Optical set-up

Targets' measurements were performed using a 532 nm MFOV lidar. Subtargets of each target category were glued on a top of a black wooden board, the later being set up at the end of the environment chamber located 105 meters from the lidar. Considering the environment chamber is 22 meters long, the target distance to the lidar was approximately 120 meters.

The lidar includes a telescope coupled to a gated intensified CCD camera (G-ICCD) synchronized with a doubled Nd-YAG laser. The laser beam is pointed at the desired location using a scene mirror and a scanner. The analyzer is a two polarized cube beam splitters and a single ICCD camera used to image simultaneously the two polarization states of the backscattered polarization (Figure 4).

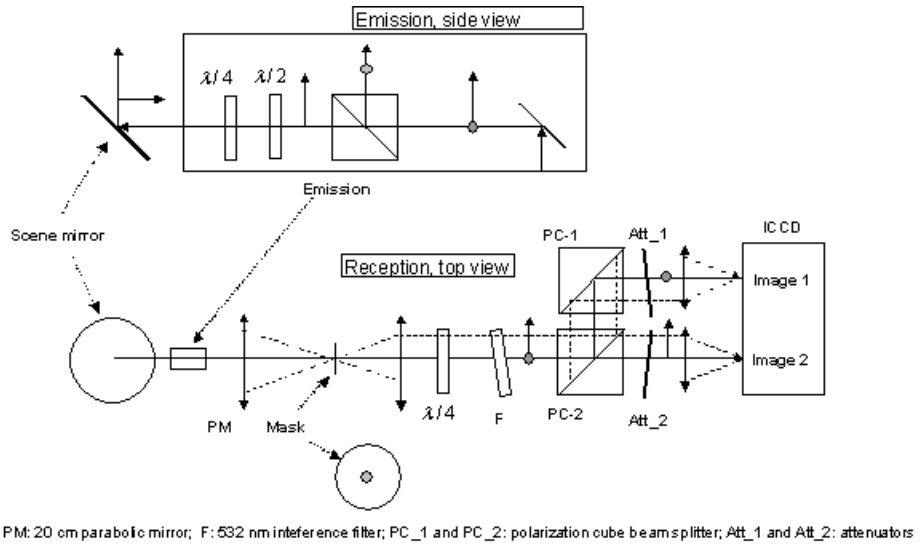

Figure 4: *Imaging the two polarization states of the backscattered*

When the polarized laser beam from the lidar hits the target, part of the light is absorbed while the other part is reflected. The backreflected lights with two components (p and s, for *parallel* and *incident* light projections) are collected and imaged by the ICCD camera, resulting in the formation of two images. A set of 1000-1000 attenuator is set up in front of the ICCD camera to attenuate the signal intensity in order to avoid the saturation of the camera's CCD chip. The light from the laser source passes through half-wave and quarter-wave retarders. Figure 5 is a schematic illustration of the optical set-up.

Both retarders could be rotated 90 $^\circ$ around their optical axis. By flipping (rotating) the half-wave and quarter-wave retarders, five (5) different polarized states of the laser light could be generated. Those were linear vertical (0 $^\circ$, 0 $^\circ$), linear horizontal

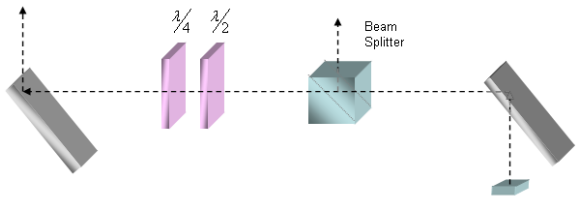

(a) Emission

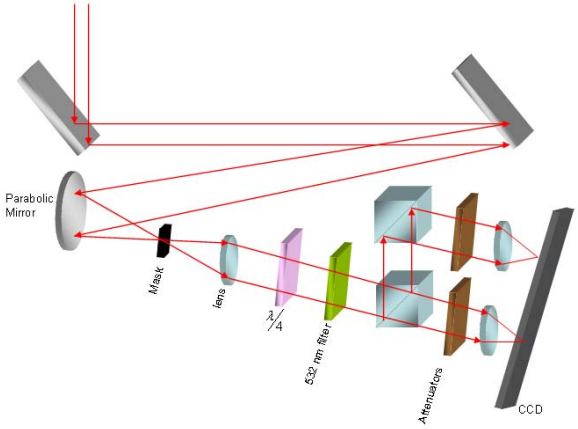

(b) Reception

Figure 5: *Schematic illustration of the optical set-up. 5(a) is the Emission layout. A laser first reflected to a beam splitter where only the parallel component is transmitted. Then, it goes through two wave-plate retarder. The half wave-plate transform the linear polarization into a circularly polarized light, while the quarter-wave plate is used to rotate the light from vertical to linear (or left to write, in the case of circular polarization). 5(b) is the Reception layout. The light from the target is reflected toward a quarter-wave plate. Then, the light is separated into two components: using two beam splitters. A CCD (an Andor i-Star Camera) acquires the two resulting images.*

$(90^\circ, 0^\circ)$, circular left $(0^\circ, \pi/2^\circ)$, circular right $(90^\circ, \pi/2^\circ)$ and *Retarders' Special* that corresponded flipping only the reception quarter-wave plate.

The backreflected light passes through a quarter-wave plate before the signal arrives to the camera. The fast axis of the wave plate is set at 0° for linearly polarized light, and at 45° for circularly polarized light to make sure the light reaching the camera is linearly polarized.

In order to illuminate the target, the laser beam divergence is increased using an external lens to the system. To examine the influence of the incident angle to target depolarization ratio and reflectivity, panels were set up and measured at desired angles. Targets made of different materials were used, including: insulations, woods,

metals, sand papers, concrete, grasses, wet and dry sands, composite plastics as well as other environmental targets with each material category (panel) containing some subtargets. Figure 6 illustrates the laser set-up.

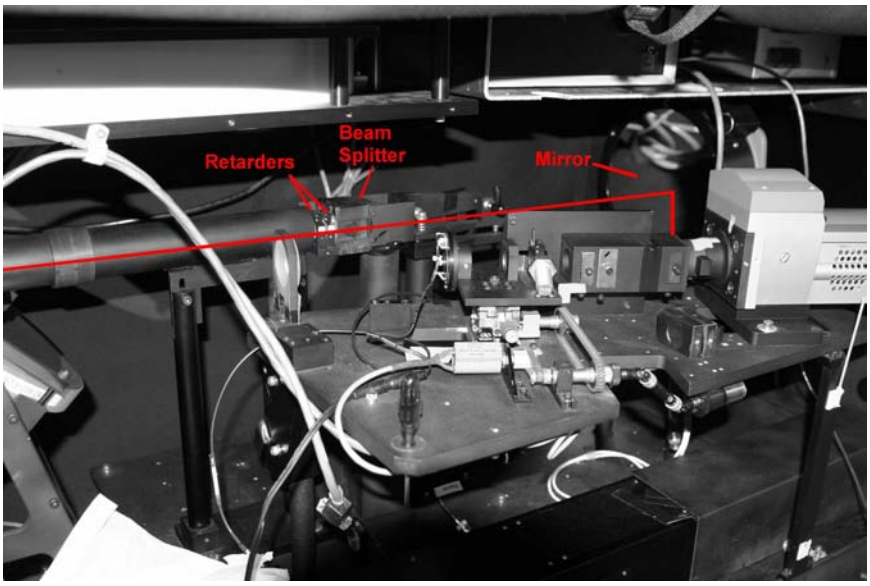

(a) Emission

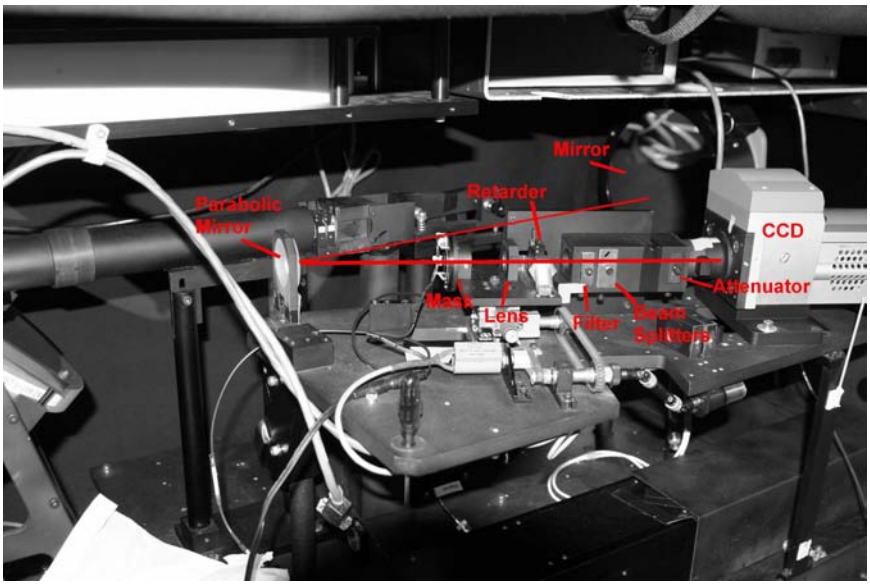

(b) Reception

Figure 6: *Laser Set-Up*

3 Methodology

The experiment was designed to examine the influence of different incident angles on the depolarization ratio of a range of solid targets. The precise measurement of the depolarization ratio requires the knowledge of the relative response of both polarization channels, and the reflectivity examination should based on uniform laser beam. Therefore, some signal calibration are necessary before further analysis.

This section presents the target acquisition and calibration acquisition methodologies used throughtout the conducted field trial.

3.1 System calibration

The lidar measurements need to be calibrated to take into account the relative response of the two polarization channels which is affected by the attenator transmission values, the mirror reflectivity difference between the s and p waves, and the signal losses in the cubes. Relative calibration (i.e. calibration to measurements of left image) of the lidar system should be performed to ensure both linear or circular depolarizations obtained are same (ideally) or close enough (in reality).

The relative factors were calculated based on the measurements of a homogeneous target with a low depolarization. The target depolarization ratio is intrinsic to the material nature and does not depend on the polarization orientation (linear vertical/horizontal or circular left/right) of the incident radiation. After the calibration, depolarization ratios resulting of linear vertically polarized light and circular polarized light can be compared between different targets.

3.2 Laser beam uniformity calibration

To illuminate most of the panel targets, large beam divergence was used: the laser beam could not be considered as being uniformly distributed. In order to be able to examine the reflectivity of each target, the non-uniformity of the laser beam has to be calibrated. This is called *laser-beam uniformity calibration*.

The laser beam calibration can be realized based on the measurements of a homogeneous target which, in the field measurement, was the subtarget supporting wooden board. For each polarized (linear horizontal and vertical, circular right and left) light, five individual measurements of the homogeneous target were averaged. The maximum value of the averaged image (right) was used as the reference to calibrate other pixels of the image. The same procedure was applied to the other image (left). The generated calibration matrix was then affected to each target category. Here is an example: Assuming the left and right image matrices of the uniform target after five

measurements averaging are M_L and M_R with element of m_{Lij} and m_{Rij}, the largest elements of the M_L and M_R being m_{Lij} and m_{Rij}, then the calibration matrices for the left and right images are:

$$C_L = M_L \cdot / m_L = \{m_{Lij}/m_L\}, \tag{1}$$

$$C_R = M_R \cdot / m_R = \{m_{Rij}/m_R\} \tag{2}$$

If the matrices of left and right images of the measuring target is T_L and T_R, then after laser beam uniformity calibration, the calibrated image matrices will be:

$$T_{L_C} = C_L \cdot \times T_L = \{c_{Lij} \cdot t_{Lij}\}, \tag{3}$$

$$T_{R_C} = C_R \cdot \times T_R = \{c_{Rij} \cdot t_{Rij}\} \tag{4}$$

Figure 7 shows comparison of image intensity of a uniform target of the wooden board before and after uniformity calibration. After the calibration, the light intensity distribution on the homogeneous target is more uniform than that without calibration.

Figure 8 illustrates an example of a panel target before and after applying the calibration procedure. Before the calibration, the lidar detected more energy from the second row targets, while after calibration the left bottom target reflected more energy. After the laser beam uniformity calibration, the target reflectivity can be examined with more reliability.

3.3 Depolarization ratio and reflectivity

The depolarization ratio (δ) of targets were calculated after relative system calibration, i.e.:

$$\delta = \frac{I_\perp}{I_\parallel} \tag{5}$$

where $I_\perp$ and $I_\parallel$ are the perpendicular energy and parallel energy received with respect to the incident laser polarization, respectively.

The camera records image of matrix size 1024×256. However, it was found that signals of the middle pixels are the most reliable to use. During the measurements, the camera system was set up recording the signals of column from 167 to 857, resulting in a matrix size 691×256, as shown in Figure 9.

The panel matrix is composed of number of submatrices representing the subtargets. The submatrix corresponding to each subtarget and its location in the panel needs to be specified before the depolarization ratio can be calculated. This part of the work was done by examination of the Andor image (as shown in Figure 9).

Since the image pixel number corresponding to the s and p components may not be the same, the energy of a unit pixel cell was used to calculate the depolarization ratio of each target. For example, for subtarget k, its depolarization ratio is:

$$\delta_i = \frac{\sum_{i,j} \left(\frac{I_\perp(i,j)}{n_{k\perp}} \right)}{\sum_{l,p} \left(\frac{I_\parallel(l,p)}{n_{k\parallel}} \right)} \tag{6}$$

where $i = i_1, ..., i_2, j = j_1, ..., j_2, l = i_3, ..., i_4, p = j_3, ..., j_4$, with $1 \leq i, l \leq 691$, $1 \leq j, p \leq 256$, and $n_{i\perp}$ and $n_{i\parallel}$ are the total pixel number covered by the subtarget image corresponding to the s and p components, respectively.

For convenience, relative reflectivity will be used, i.e. the ratio energy received from target k to that from target of white Spectralon. Thus, the relative reflectivity is the reflectivity relative to the white Spectralon at each incident angle:

$$R_i = \frac{I_i(tot)}{I_r(tot)} = \frac{\frac{I_{i\perp}(tot)}{n_{i\perp}} + \frac{I_{i\parallel}(tot)}{n_{i\parallel}}}{\frac{I_{r\perp}(tot)}{n_{r\perp}} + \frac{I_{r\parallel}(tot)}{n_{r\parallel}}} \tag{7}$$

where $I_r(tot)$ is the unit pixel cell total energy received from the reference target r (white Spectralon), and $I_i(tot)$ is the unit pixel cell total energy received from the subtarget i.

3.4 Target acquisition

Multi-target boards were set up at four different angles (0°, 15°, 30°, 45°). Then, five polarized states (linear vertical, linear horizontal, circular left and circular right and *Retarders' Special*) were used. Since the depolarization results are based on the average counts, five images were acquired for each polarization state limiting the measuring noise. Therefore, twenty-five images were acquired at each angle and one hundred images were used for one set. Due to the small laser beam, the multi-target was then turned upside down so the second half of the target could be measured.

Figure 10 shows the position of each retarder during a measurement set.

The acquisition procedure can be summarized as follows:

1. Install the wood panel with the subtargets to be measured;
2. Set the angle;
3. Acquire five images illuminated with vertical linear polarized light source;

4. Acquire five images illuminated with horizontal linear polarized light source;
5. Acquire five images illuminated with circular left polarized light source;
6. Acquire five images illuminated with circular right polarized light source;
7. Acquire five images illuminated with *Retarders' Special* montage;
8. Set another angle.

3.5 Calibration acquisition

In order to illuminate the top half of the target, the laser divergence was increased. This produced a non-uniform illumination (Gaussian-type) over the target. To compensate this effect, the return signal was measured previously without the target in place. A black wooden board acted as a uniform target. As with the target acquisition process, five images were acquired for each polarization state and incident angle. This calibration is possible if one suppose the backscattered signals from the bare board to be the same as the multi-target board.

The calibration procedure was carried out every two targets since the laser beam signal drifted with time.

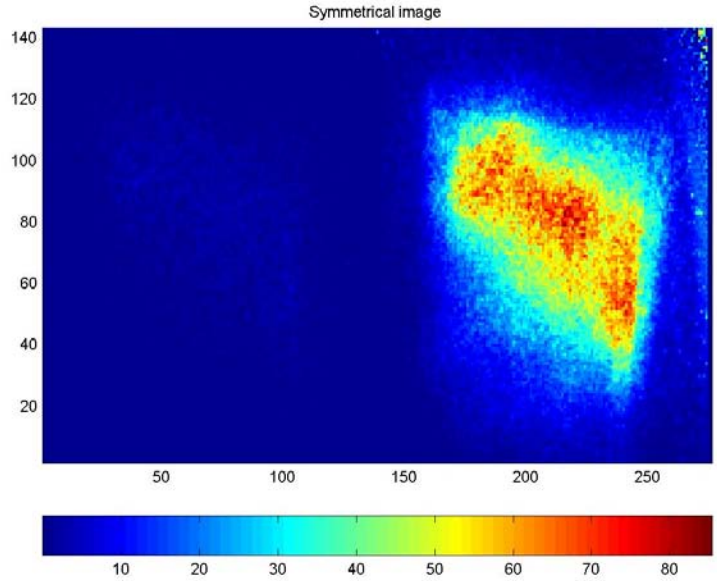

(a) Before calibration

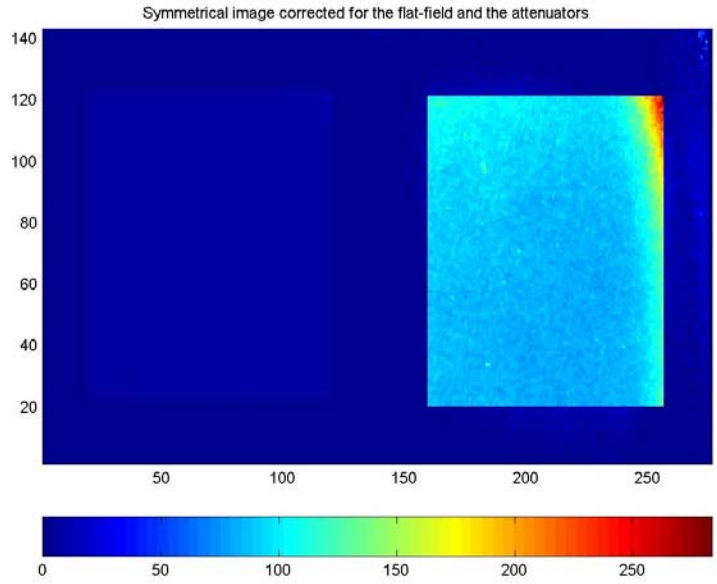

(b) After calibration

Figure 7: *Comparison of image intensity of a uniform target 7(a) before and 7(b) after laser beam uniformity calibration.*

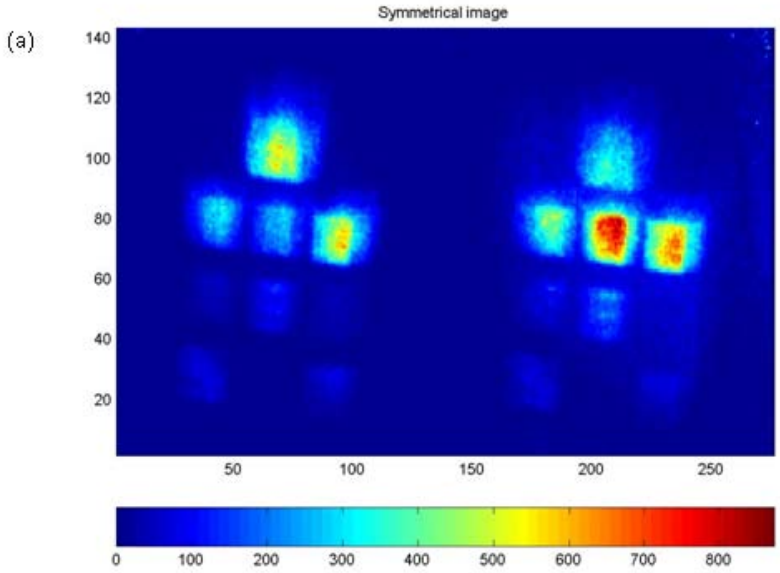

(a) Before calibration

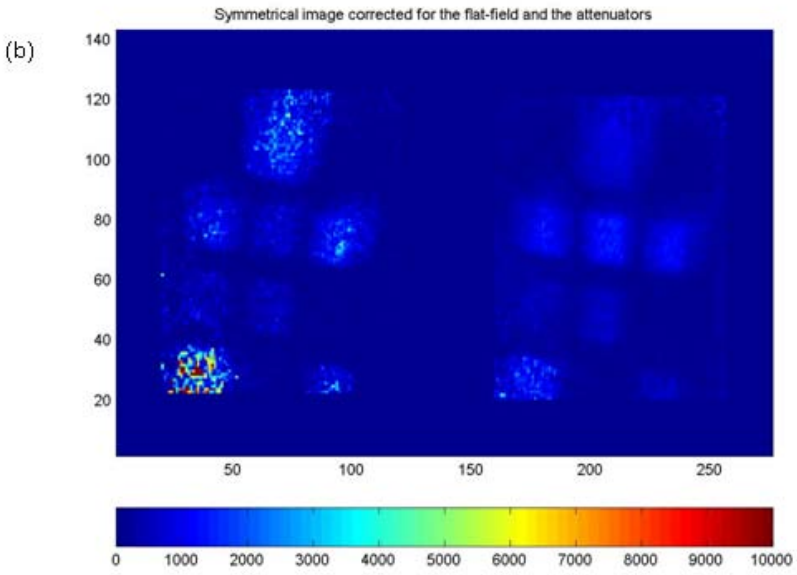

(b) After calibration

Figure 8: *Comparison of images of a panel with subtargets 8(a) before and 8(b) after laser beam uniformity calibration.*

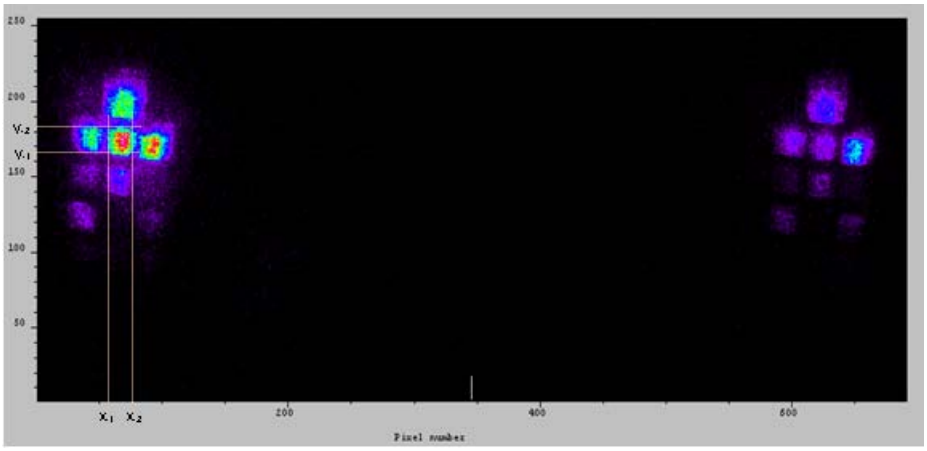

Figure 9: *Locating subtargets*

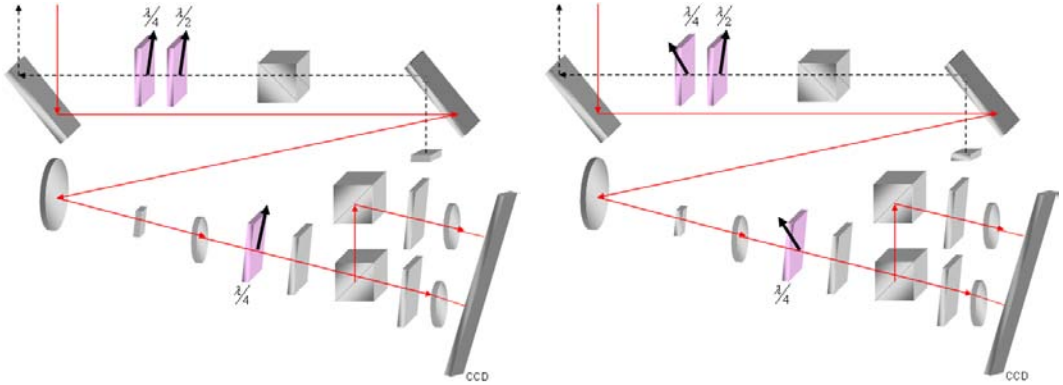

(a) Linear Vertical

(b) Linear Horizontal

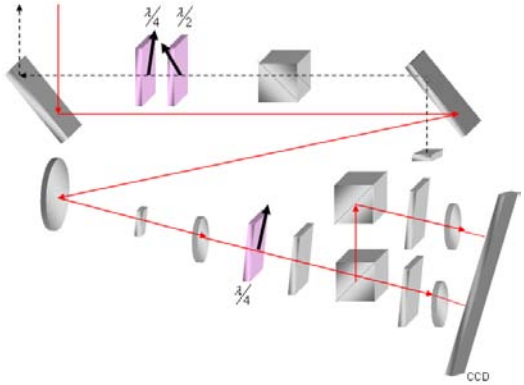

(c) Circular Left

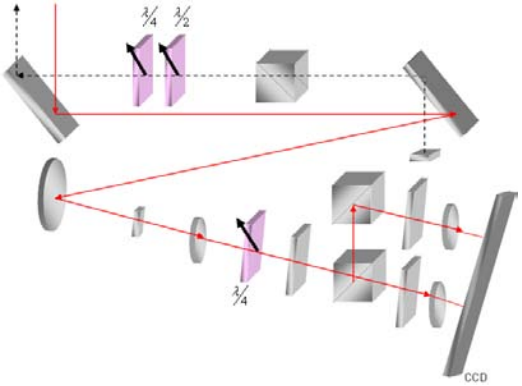

(d) Circular Right

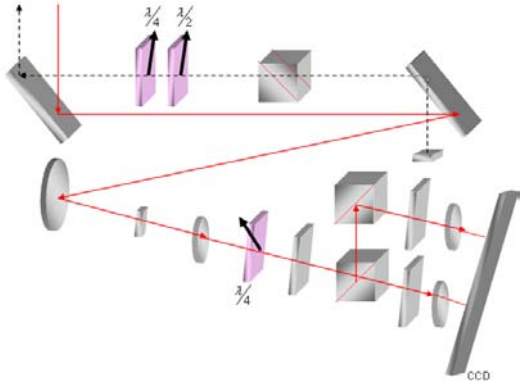

(e) *Retarders'Special*

Figure 10: *Position of the retarder for each polarization state*

4 Acquisition of polarimetric signatures from solid targets

Different materials were used as solid targets; they are categorized as insulations, woods, metals, sand papers, concrete, grasses, wet/dry sands, composite plastics, and environmental targets. These solid targets will be analyzed and discussed one by one wrt their category.

The targets were installed on two wooden boards. The backward is measuring 20" x 40". At its top were installed two Spectralons: a black one and a white one. On the right side, there was a black painted spot. All these three squares were used as references. The forward wood panel is measuring 20" x 32" with subtargets measuring 4" x 4". The wood panel was painted in black to reduce the reflection.

The multi-target boards were divided into eight different groups:

1. Insulations
2. Woods
3. Metals
4. Environments
5. Sand papers
6. Composite plastics
7. Bottles
8. Sands

For the convenience of comparison, the first three targets within a board were always located at the top of each panel.

4.1 Insulation targets on panel 1

The first multi-target board was mainly composed of Styrofoam™. Figure 11 illustrates the board and Table 1 presents the different insulation materials and position of the center of panel 1.

4.1.1 Depolarization ratio

Figure 12 illustrates the influence of incident angle on the depolarization ratio. Table 2 presents the depolarization ratios analysis results of insulation targets on panel 1. It is found that circular polarization ratio δ_c is about twice the value of linear polarization ratio δ_L for almost all insulation targets (Figure 12).

Table 1: *Insulation targets and position of the center*

No	On the list	English Name	Center	
			x (cm)	y (cm)
1	Vive	Empty		
2	Spectralon blanc	White spectralon	25.4	6.75
3	Spectralon noir	Black spectralon	44.45	6.75
4	Styrofoam bleu	Blue extruded polystyrene (Styrofoam™)	10	-6.5
5	Styrofoam Rose	Pink extruded polystyrene (Styrofoam™)	26	-6.5
6	Styrofoam blanc	White extruded polystyrene (Styrofoam™)	41.5	-6.5
7	Mousse à l'uréthane	Polyuréthane foam insulation	10	-22
8	Styro-mousse blanc	White Styrofoam™	26	-22
9	Styro-mousse: noir	Black Styrofoam™	41.5	-22
10	Réflectik™	Reflectik™	10	-37.5
11	Styro-mousse noir léger	Black light Styrofoam™	26	-37.5
12	Styro-mousse beige	Brown Styrofoam™	41.5	-37.5
13	Mini bull transparente	Transparent mini-bubble	10	-54.5
14	Laine anti-feu	Fireproof wool	26	-54.5
15	Laine rose horizontal	Horizontal mineral wool	41.5	-54.5

Based on Table 2, and Figure 12(a), it is found that target 12 (*brown Styrofoam*) showed the largest linear depolarization ratio of value about 0.6 at any incident angles. The other insulation targets showed comparative values to target 2 (*white Spectralon*), with linear depolarization ratios between 0.3 and 0.5. Exceptions are targets 9 and 11 (*black Styrofoam* and *black light Styrofoam*) which showed smaller linear depolarization ratios than the others.

Incident angle showed largest influence on target 13 (*transparant mini-bubble*): there was almost no depolarization at angle 0 $^\circ$, but the linear depolarization ratio almost doubled every 15 $^\circ$ increase from 0 $^\circ$ to 30 $^\circ$. It is also found that depolarization ratios of insulation tragets increase with incident angle, with a few exceptions. Fost most insulation targets, the increase of depolarization ratio with incident angle mainly showed up when incident angle was small. The larger the incidence angle, the less change or even opposite change to the depolarization ratio. Targets 9 (*black Styrofoam*) and 11 (*black light Styrofoam*) showed very close depolarization properties: they are both Styrofoam with dark colors.

The change of circular depolarization ratio incident angle showed similar trends as linear ones. However, it is the circular depolarization ratio of target 10 (*rflectik*) rather than target 12 (*brown Styrofoam*) as for the linear depolarization ratio that showed the largest value among all other insulation targets. Indeed, the ratio $\frac{\delta_C}{\delta_L}$ of target 10 (*reflectik*) has a value of 3 rather than 2 for the other targets. Both linear and circular depolarization ratios of target 3 (*black Spectralon*) increased significantly

Table 2: *Depolarization ratios of insulation targets of panel 1*

Target #	Depolarization ratio							
	δ_L				δ_C			
	0 °	15 °	30 °	45 °	0 °	15 °	30 °	45 °
1	0.10	0.12	0.14	0.16	0.27	0.32	0.36	0.43
2	0.44	0.51	0.47	0.50	1.27	1.49	1.43	1.58
3	0.17	0.31	0.24	0.24	0.40	0.73	0.59	0.68
4	0.41	0.46	0.53	0.58	0.73	0.83	0.91	1.07
5	0.23	0.26	0.36	0.41	0.36	0.44	0.65	0.82
6	0.59	0.46	0.48	0.54	0.88	0.70	0.73	0.91
7	0.30	0.37	0.36	0.32	0.49	0.62	0.61	0.61
8	0.35	0.36	0.43	0.45	0.56	0.59	0.67	0.69
9	0.22	0.24	0.21	0.22	0.51	0.60	0.48	0.59
10	0.37	0.47	0.49	0.42	1.03	1.45	1.63	1.43
11	0.19	0.27	0.26	0.20	0.41	0.56	0.54	0.48
12	0.61	0.68	0.63	0.60	0.83	1.04	1.03	0.97
13	0.07	0.17	0.31	0.37	0.46	0.74	0.96	0.93
14	0.30	0.30	0.31	0.33	0.64	0.65	0.67	0.71
15	0.32	0.32	0.43	0.42	0.62	0.61	0.79	0.75

with incident angle.

4.1.2 Relative reflectivity

Table 3 shows analysis results of relative reflectivity of insulation targets on panel 1.

Figure 13 is the corresponding chart showing influence of incident angle on relative reflectivity of insulation targets. Relative reflectivity of targets 9 (*black Styrofoam*) and 11 (*black light Styrofoam*) are close to each other, and remained the smallest among all the insulation materials being examined in this research. Moreover, they are very close to the reference target of black Spectralon. Relative reflectivity of most insulation targets decreased with incident angle, with the exception of target 10 (*reflectik*) whose relative reflectivity increased dramatically from 0 ° to 15 °. When the incident angle further increased, the relative reflectivity of target 10 followed the same trend as the other insulation targets, and decreased with the incident angle. Based on figure 13, the reflectivity sequence of targets in panel 1 in decrease order is: $10 \rightarrow 6 \rightarrow 4 \rightarrow 12 \rightarrow 5 \rightarrow 2 \rightarrow 8 \rightarrow 7 \rightarrow 15 \rightarrow 14 \rightarrow 13 \rightarrow 9 \rightarrow 11 \rightarrow 3 \rightarrow 1$. This expresses the fact that the lighter the color of the insulation target, the more energy is being reflected.

When relative reflectivities are related to their corresponding depolarization ratios, it is found that insulation targets having higher reflectivity usually shows higher relative depolarization too, and vice versa (Figure 14). The depolarization ratios at larger incident angles appeared to follow more the trend than at smaller incident angles. Figure 14 also indicates that the depolarization ratios at higher incident angles are

Table 3: *Relative reflectivity of targets of panel 1*

Target #	Relative reflectivity							
	δ_L				δ_C			
	0 °	15 °	30 °	45 °	0 °	15 °	30 °	45 °
1	0.08	0.07	0.06	0.06	0.09	0.08	0.07	0.07
2	1.00	1.00	1.00	1.00	1.00	1.00	1.00	1.00
3	0.11	0.10	0.06	0.07	0.11	0.09	0.06	0.08
4	2.17	1.92	1.51	1.15	1.68	1.33	1.15	1.25
5	1.69	1.29	1.01	0.75	1.45	1.02	0.78	0.92
6	2.56	2.25	2.00	1.81	1.94	1.60	1.31	1.77
7	0.98	0.81	0.70	0.76	0.74	0.54	0.62	0.77
8	1.03	1.02	0.76	0.86	0.81	0.65	0.63	0.86
9	0.24	0.25	0.22	0.24	0.20	0.19	0.18	0.28
10	1.09	2.85	2.07	1.90	1.84	2.29	2.19	2.05
11	0.19	0.19	0.16	0.24	0.20	0.14	0.17	0.22
12	2.09	1.92	1.35	1.63	1.10	1.12	1.18	1.53
13	0.59	0.41	0.22	0.26	1.14	0.43	0.25	0.30
14	0.66	0.53	0.44	0.50	0.59	0.45	0.44	0.53
15	0.78	0.81	0.61	0.64	0.72	0.59	0.55	0.62

usually larger than those at smaller angles. However, the depolarization ratio is not truly function of the reflectivity since insulation targets with the highest reflectivity do not necessary have the largest depolarization ratio. Therefore, the depolarization ratio should be related to other properties of the targets.

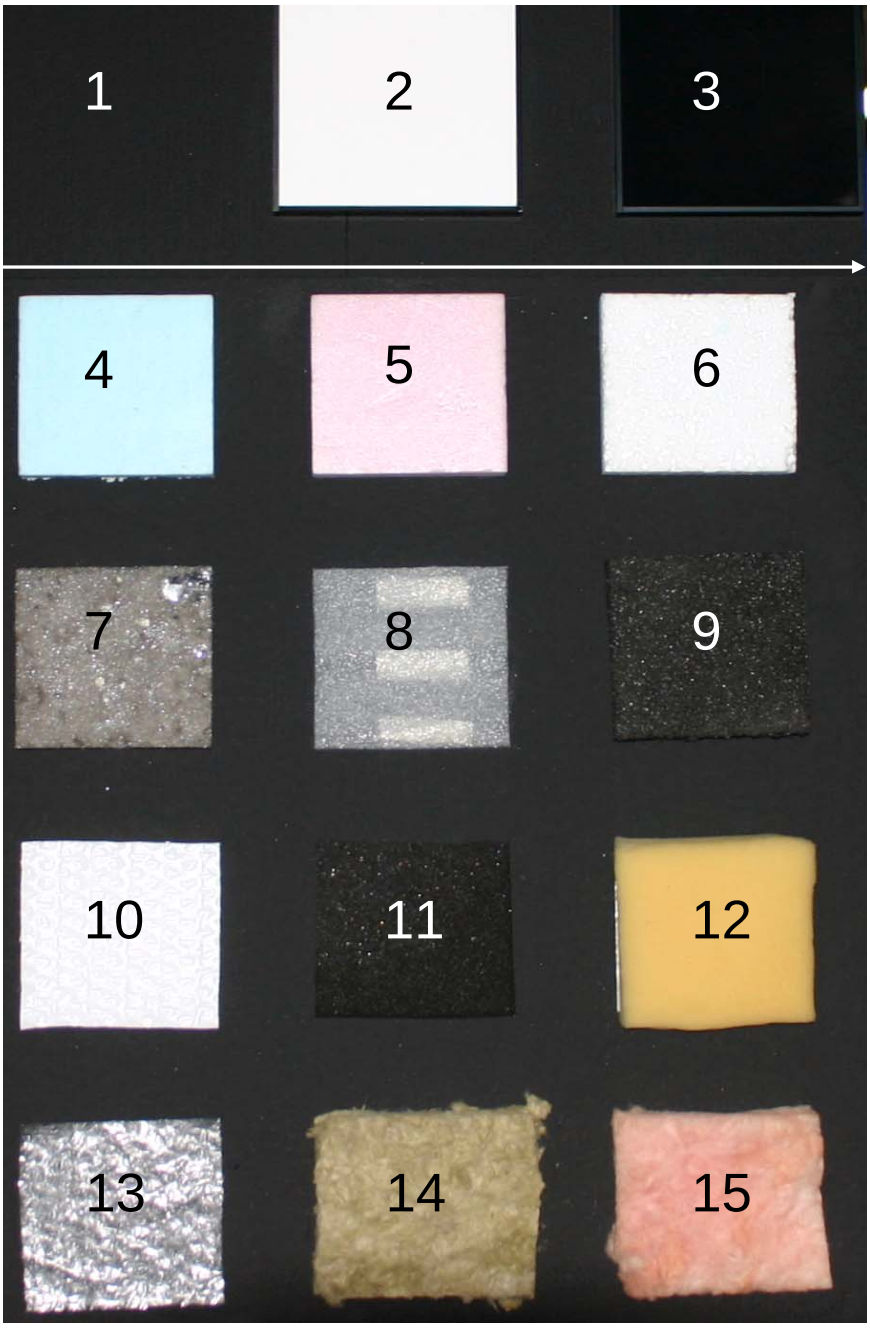

Figure 11: *Layout of insulation targets*

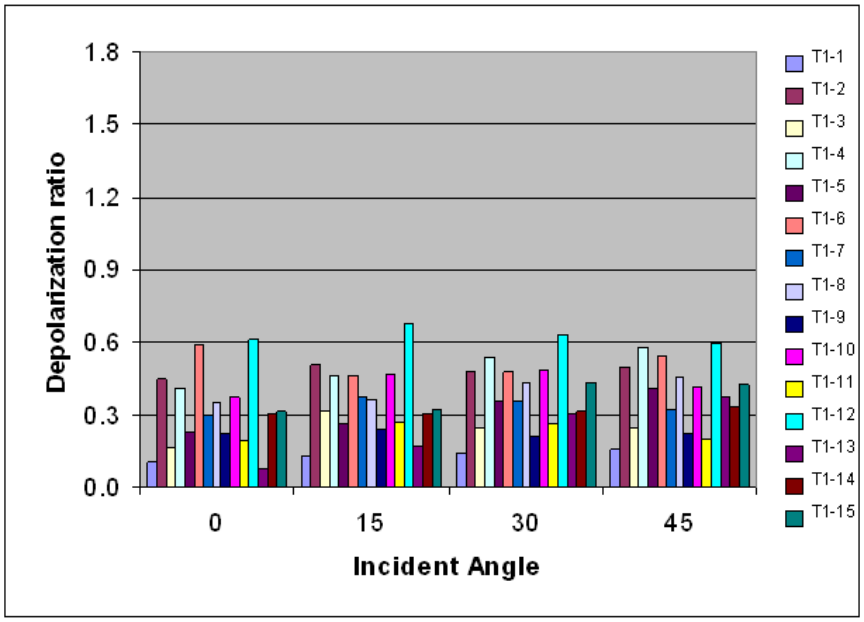

(a) Linear depolarization ratio (δ_L)

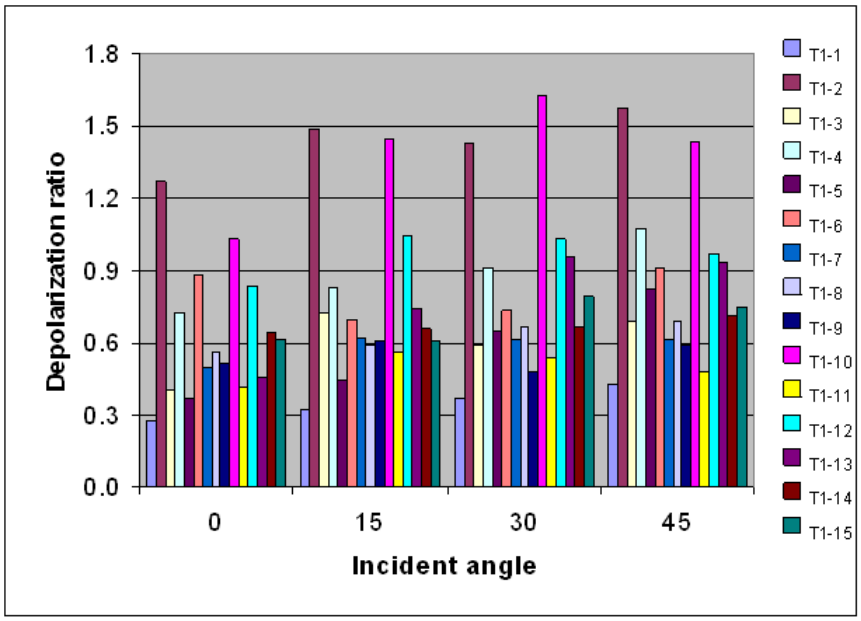

(b) Circular depolarization ratio (δ_C)

Figure 12: *Depolarization ratio change with incident angle for insulation targets. 12(a) linear depolarization ratio, and 12(b) circular depolarization ratio.*

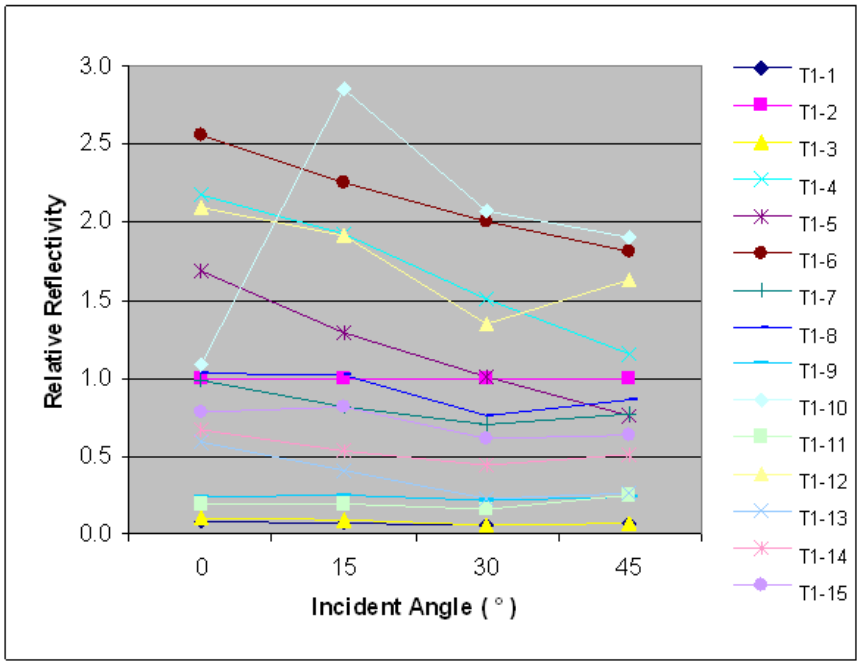

(a) Linear relative reflectivity

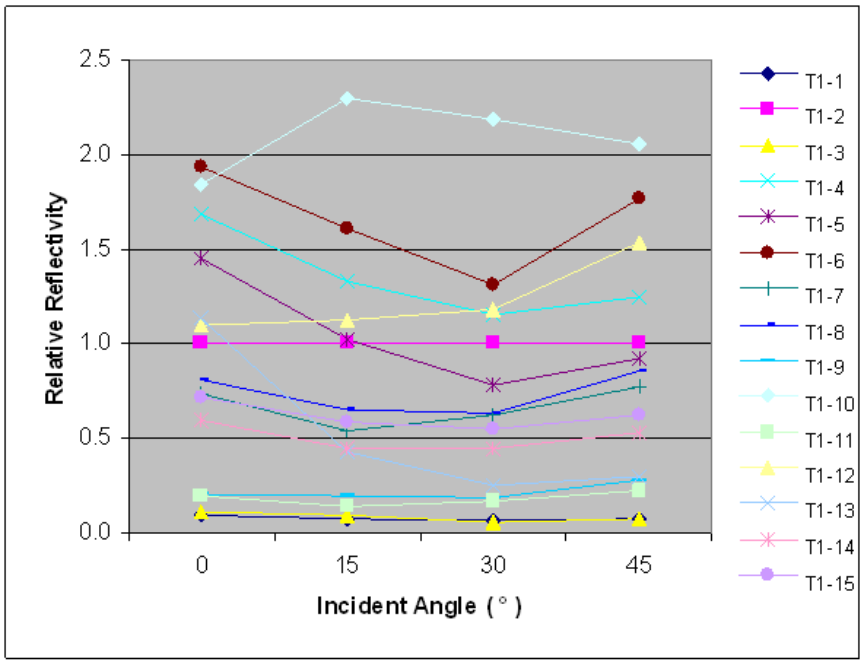

(b) Circular relative reflectivity

Figure 13: *Relative reflectivity change with incident angle for insulation targets. 13(a) linear relative reflectivity, and 13(b) circular relative reflectivity.*

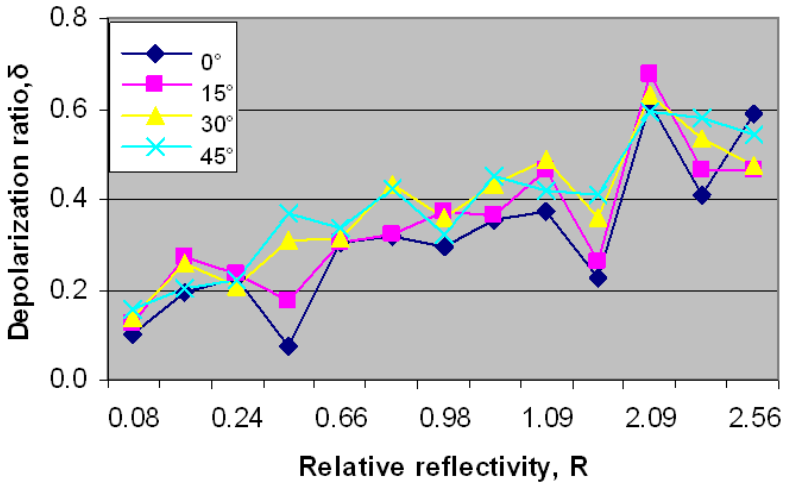

Figure 14: *Relationship between depolarization ratio and reflectivity of insulation targets.*

4.2 Wood targets

The materials of applied wood targets are listed in Table 4. The arrangement of the targets is shown in Figure 15.

The following subsections present the depolarization ratios and relative reflectivity analysis results following measurements conducted on these wood targets.

Table 4: *Wood targets and position of the center*

No	On the list	English Name	Center Position	
			x (cm)	y (cm)
1	Vide	Empty		
2	Spectralon blanc	White spectralon	25.4	6.75
3	Spectralon noir	Black spectralon	44.45	6.75
4	Pins	Pine	10	-6.5
5	Épinette	Spruce	26	-6.5
6	Merisier	Cherry birch	41.5	-6.5
7	Chêne	oak	10	-22
8	Contreplaqué horizontal	Horizontal plywood	26	-22
9	Contreplaqué vertical	Vertical plywood	41.5	-22
10	OSB	Oriented strand board	10	-37.5
11	"Ripe pressé" standard	Rip board	26	-37.5
12	Cèdre	Cedar	41.5	-37.5
13	Papier noir	Black paper	10	-54.5
14	Bardeaux d'asphalte	Asphalt shingles	26	-54.5
15	Vide	Empty	41.5	54.5

4.2.1 Depolarization ratio

The corresponding analysis results of depolarization ratios and their change with incident angle are shown in Table 5 and illustrated in Figure 16.

It is found that these targets can be grouped into three categories based on the depolarization ratios and wrt their with incident angle. One is $\{4, 5, 9, 10, 11\}$ with depolarization ratio around 0.345. The second group is $\{6, 8\}$ which showed fast increase rate from 0° to 15°, then remained value around 0.45. The third group is $\{7, 12, 14\}$ with depolarization ratio of about 0.25. The last one with the smallest depolarization is target 13 (*black paper*).

Figure 16 illustrates that all targets have smaller depolarization ratios than target 2 (*white Spectralon*). Indeed, the depolarization ratios of most wood targets increased with incident angle, no matter if it is linear or circular one. However, there is an exception with target 9 (*vertical plywood*) as its depolarization decreased with the incident angle when the later one is greater than 15°. A reason for this might be caused by some measurement noise induced. Note that most circular depolarization ratios are $2.5 \sim 3.5$ times the value of linear ones.

Table 5: *Depolarization ratios of wood targets*

Target #	Depolarization ratio							
	δ_L				δ_C			
	0 °	15 °	30 °	45 °	0 °	15 °	30 °	45 °
1	0.09	0.12	0.14	0.18	0.24	0.30	0.36	0.43
2	0.46	0.50	0.50	0.47	1.34	1.47	1.46	1.52
3	0.19	0.20	0.22	0.25	0.42	0.47	0.55	0.65
4	0.33	0.35	0.38	0.37	1.07	1.13	1.26	1.24
5	0.32	0.30	0.32	0.33	1.09	1.04	1.17	1.26
6	0.28	0.42	0.42	0.45	1.05	1.42	1.38	1.53
7	0.22	0.28	0.30	0.29	0.99	1.15	1.18	1.16
8	0.33	0.42	0.47	0.41	1.25	1.47	1.50	1.44
9	0.36	0.39	0.35	0.31	1.35	1.34	1.33	1.19
10	0.32	0.31	0.36	0.34	1.08	1.07	1.21	1.24
11	0.35	0.35	0.38	0.36	0.97	0.99	1.14	1.24
12	0.21	0.24	0.23	0.25	0.78	0.93	0.98	1.08
13	0.07	0.10	0.15	0.19	0.18	0.26	0.41	0.49
14	0.25	0.25	0.27	0.25	0.67	0.70	0.77	0.75
15	0.07	0.10	0.12	0.14	0.18	0.25	0.29	0.36

4.2.2 Relative reflectivity

Reflectivity of each target was examined relative to the reflectivity of white Spectralon. Figure 17 compares the relative linear and circular reflectivity of wood targets. Detailed analysis results is presented in table 6.

Unlike the panel 1 (insulation) targets that showed relative reflectivity values decreased with the incident angle, most panel 2 (wood) targets showed linear relative reflectivity increasing with the incident angle. Exception is target 10 (*oriented strand board*) whose relative reflectivity decreased by half value from 0 ° to 15 °. The relationship between relative circular reflectivity and the incident angle is not obvious. Indeed, some results showed initially very large reflectivity, then dropped sharply afterward. This might be due to the imperfect laser beam uniformity calibration, resulting in overcalibrated signals. Moreover, when the incident angle was small, the energy received from circulated polarized light is usually at least twice more than those from linear polarized light. However, they are getting closer to each other when incident angle increased.

No wood targets has reflectivity greater than white Spectralon. Amid all the wood targets, target 13 (*black paper*) and target 15 (*empty*) showed smallest reflectivity because both of them are black, followed by target 14 (*asphalt shingles*) whose also of dark color.

Surprisingly, target 6 (*cherry birch*) and target 9 (*vertical plywood*) showed very small reflectivity at 0 ° and 15 ° incident angles when incident light is linearly polarized,

Table 6: *Relative reflectivity results of wood targets*

Target #	Relative reflectivity							
	δ_L				δ_C			
	0 °	15 °	30 °	45 °	0 °	15 °	30 °	45 °
1	0.05	0.04	0.04	0.04	0.06	0.05	0.04	0.04
2	1.00	1.00	1.00	1.00	1.00	1.00	1.00	1.00
3	0.07	0.06	0.05	0.06	0.08	0.05	0.04	0.06
4	0.27	0.34	0.39	0.47	0.45	0.47	0.32	0.32
5	0.24	0.47	0.42	0.51	0.52	0.85	0.38	0.43
6	0.03	0.07	0.38	0.36	0.07	0.21	0.33	0.28
7	0.30	0.42	0.35	0.47	0.60	0.68	0.32	0.36
8	0.18	0.25	0.43	0.48	0.42	0.64	0.35	0.36
9	0.03	0.04	0.37	0.52	0.05	0.14	0.42	0.45
10	0.43	0.21	0.22	0.27	0.35	0.27	0.27	0.30
11	0.21	0.19	0.17	0.18	0.26	0.24	0.19	0.16
12	0.21	0.19	0.19	0.24	0.32	0.25	0.22	0.22
13	0.05	0.02	0.02	0.02	0.06	0.03	0.02	0.02
14	0.25	0.06	0.07	0.09	0.07	0.07	0.08	0.09
15	0.03	0.03	0.03	0.04	0.04	0.04	0.03	0.03

compared with other wood targets in light color. Nevertheless, when incident angle increased from 30 ° to 45 °, they caugh up with other targets in similar light color. When the cirular polarized light was used, similar results showed up except that reflectivity of target 6 (*cherry birch*) and target 9 (*vertical plywood*) are more clear from 0 ° to 15 °.

The depolarization ratio increased faintly with reflectivity. However, the trend is not as clear as for panel 1 (insulation) targets, especially for those targets with smallest reflectivity but relatively largest depolarization, as shown in Figure 18. Still, for most wood targets, the depolarization ratio at larger incident angle is greater than that of smaller incident angle.

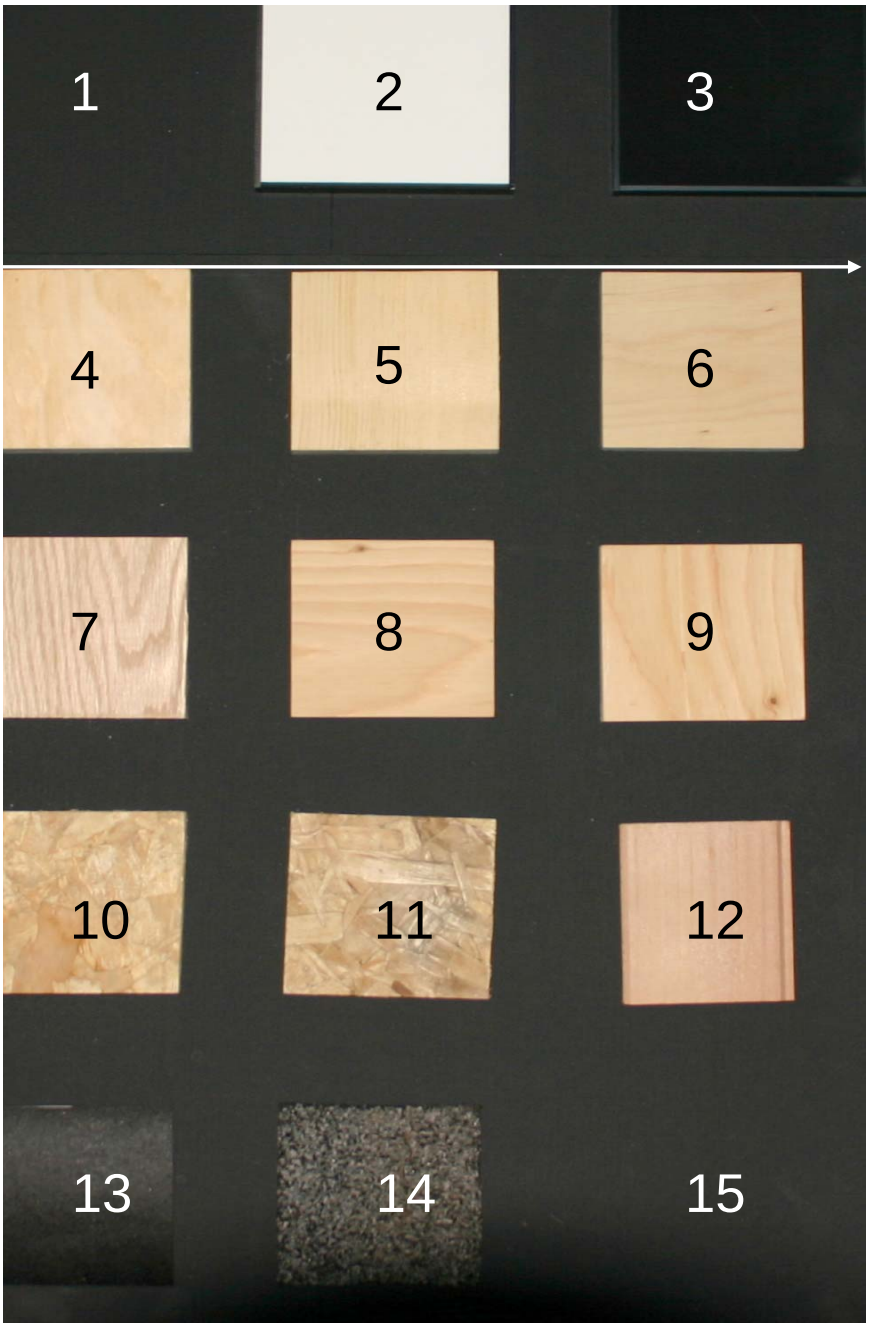

Figure 15: *Loyaout of wood targets*

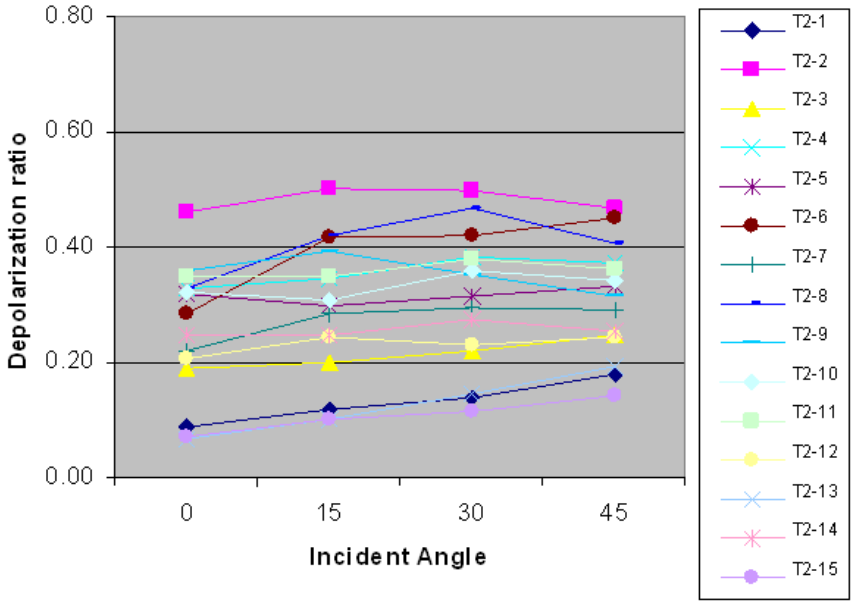

(a) Linear depolarization ratio (δ_L)

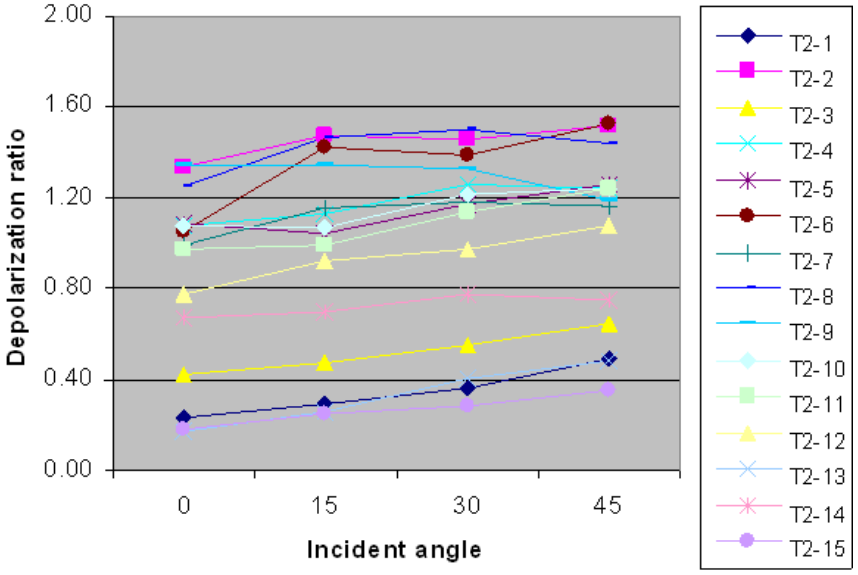

(b) Circular depolarization ratio (δ_C)

Figure 16: *Depolarization ratios of wood targets and their change with incident angle. 16(a) linear depolarization ratio, and 16(b) circular depolarization ratio.*

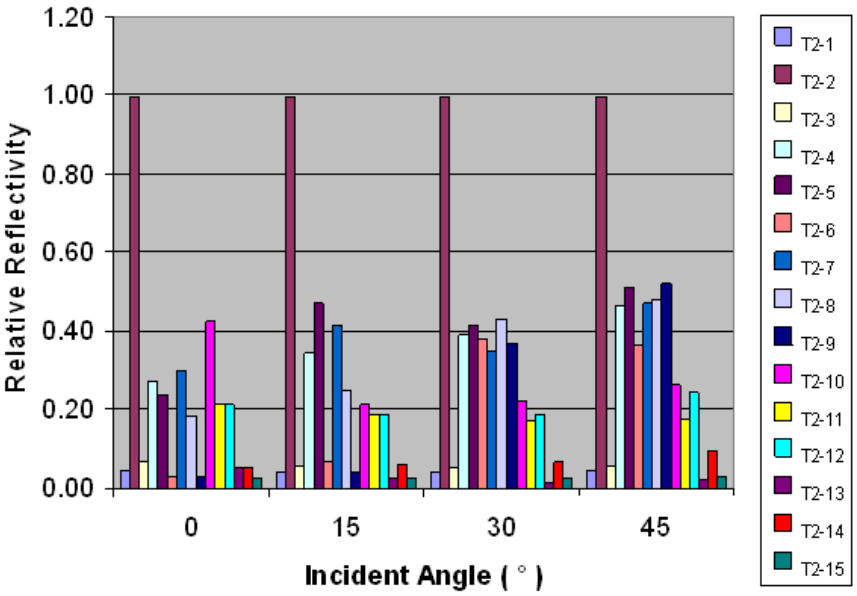

(a) Relative linear reflectivity

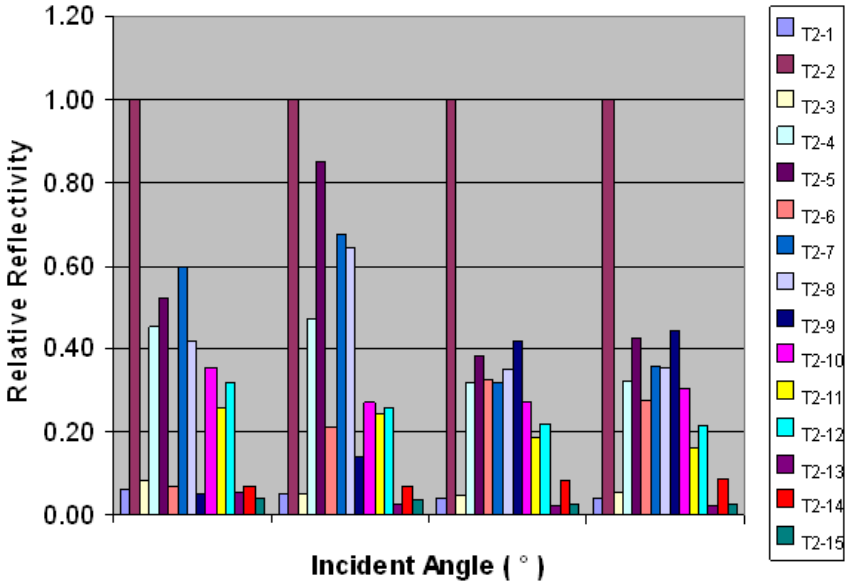

(b) Relative circular reflectivity

Figure 17: *Relative 17(a) linear reflectivity, and 17(b) circular reflectivity of wood targets.*

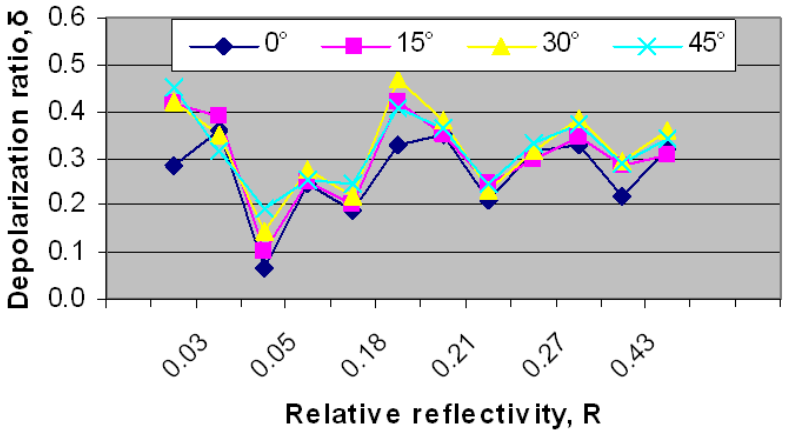

Figure 18: *Relationship between depolarization ratio and reflectivity of wood targets.*

4.3 Metallic targets

Numerous metallic targets were glued on a black board as shown in Figure 19. The description of each metallic target is described in Table 7.

Table 7: *Metallic targets and position of the center*

No	On the list	English Name	Center Position	
			x (cm)	y (cm)
1	Vide	Empty		
2	Spectralon blanc	White spectralon	25.4	6.75
3	Spectralon noir	Black spectralon	44.45	6.75
4	Stainless vertical	Vertical stainless steel	10	-6.5
5	Stainless horizontal	Horizontal stainless steel	26	-6.5
6	Acier vert forêt	Green forest steel	41	-6.5
7	Cuivre	Copper	10	-22
8	Acier galvanisé	Galvanized steel	26	-22
9	Acier vert pâle	Light green steel	41.5	-22
10	Laiton	Brass	10	-37.5
11	Aluminium	Aluminum	26	-37.5
12	Acier "sand-blasté"	Sandblasted steel	41.5	-37.5
13	Acier naturel	Natural steel	10	-54.5
14	Batterie 6 volts Duracell™	6-volts batteries (Duracell™)	26	-54.5
15	Laine d'acier	Steel wool	41.5	-54.5

The following subsections present the depolarization ratios and relative reflectivity analysis results following measurements conducted on these metallic targets.

4.3.1 Depolarization ratio

Figure 20 illustrates the depolarization ratios change of these metallic targets with incident angle. Depolarization ratios increased with the incident angle approximately linearly for most of the metallic targets. As it was the case with targets of panel 2 (wood), metallic targets in panel 3 can be categorized into two groups: {6, 9} and {4, 5, 7, 8, 10, 11, 12, 13, 14, 15}. Target 6 (*green forest steel*) and target 9 (*light green steel*) showed depolarization ratios twice as large as for the other metallic targets. For all these targets, the depolarization ratios at incident angle 0° are very smaller. There were some raise of depolarization ratios as incident angle increase, but most of them are still lower than 0.15 with the exception of target 6 (*green forest steel*) and target 9 (*light green steel*) which are both colored in green. Note that the depolarization ratios of metallic targets are even smaller than target 3 (*black Spectralon*), and that circular depolarization ratios are usually $2.5 \sim 3.0$ times of the linear ones.

Analysis results of depolarization ratios for metallic targets are shown in Table 8.

Table 8: *Depolarization ratio of metallic targets*

Target #	Depolarization ratio							
	δ_L				δ_C			
	0 °	15 °	30 °	45 °	0 °	15 °	30 °	45 °
1	0.05	0.08	0.09	0.12	0.16	0.20	0.28	0.31
2	0.42	0.51	0.50	0.48	1.11	1.47	1.52	1.52
3	0.09	0.14	0.20	0.25	0.18	0.32	0.50	0.76
4	0.02	0.04	0.04	0.07	0.07	0.11	0.17	0.35
5	0.01	0.05	0.10	0.16	0.06	0.19	0.27	0.41
6	0.07	0.19	0.33	0.32	0.19	0.51	1.04	1.10
7	0.02	0.07	0.09	0.13	0.06	0.18	0.24	0.36
8	0.01	0.03	0.11	0.14	0.04	0.09	0.29	0.42
9	0.06	0.23	0.28	0.37	0.15	0.66	0.86	1.30
10	0.01	0.03	0.07	0.11	0.04	0.12	0.21	0.33
11	0.01	0.03	0.08	0.10	0.04	0.11	0.20	0.32
12	0.03	0.04	0.11	0.13	0.06	0.13	0.26	0.39
13	0.01	0.02	0.06	0.09	0.05	0.08	0.15	0.26
14	0.01	0.04	0.09	0.12	0.04	0.12	0.24	0.32
15	0.06	0.07	0.10	0.14	0.13	0.20	0.23	0.31

4.3.2 Relative reflectivity

Figure 21 illustrates the relative reflectivity values of different metallic targets while Table 9 describes the analysis results. The Reflectivity of metallic targets greatly decreased when incident angle changed from 0 ° to 15 ° . The highest the reflectivity, the more abrupt the change of reflectivity. When incident angle further increased, the reflectivity decreased but with small decreased rates. This is illustrated by targets 7 (*copper*), 8 (*galvanized steel*), 10 (*brass*), and 11 (*aluminum*). The influence of the incident angle to less reflective metallic targets is very small: their reflectivity remained mostly unchanged as it is the case for target 1 (*empty*) and target 3 (*black Spectralon*) when the incident angle increased. Note that similarly to the wood targets, circular reflectivity at 0 ° incident angle was about twice the value of the one from linear reflectivity; the difference decreased as the incident angle increased.

Metals are special targets that hardly relates depolarization ratio and reflectivity. Based on the results at incident angle 0 ° , it seems tjat the depolarization ratios of metallic targets decreased slightly with the targets' reflectivity. Generally, the change is so small that the reflectivity has little influence on the depolarization ratio, as shown in Figure 22. For most metallic targets, depolarization ratio increased with the incident angle.

Table 9: *Relative reflectivity results of metallic targets*

Target #	Relative reflectivity							
	δ_L				δ_C			
	0 °	15 °	30 °	45 °	0 °	15 °	30 °	45 °
1	0.07	0.07	0.09	0.07	0.11	0.10	0.09	0.07
2	1.00	1.00	1.00	1.00	1.00	1.00	1.00	1.00
3	0.08	0.05	0.10	0.07	0.11	0.06	0.10	0.07
4	0.29	0.26	0.25	0.17	0.54	0.30	0.27	0.18
5	0.99	0.14	0.11	0.08	1.77	0.17	0.10	0.07
6	0.42	0.32	0.25	0.19	0.69	0.33	0.22	0.17
7	1.24	0.43	0.39	0.33	2.15	0.46	0.36	0.27
8	8.29	0.97	0.36	0.27	14.08	1.12	0.37	0.23
9	0.92	0.73	0.70	0.91	1.51	0.79	0.67	0.66
10	4.56	0.35	0.15	0.09	7.24	0.41	0.16	0.08
11	3.02	0.19	0.10	0.08	5.27	0.22	0.11	0.08
12	1.82	1.18	0.36	0.27	2.46	0.72	0.39	0.23
13	0.86	0.17	0.08	0.04	1.30	0.18	0.08	0.08
14	0.77	0.12	0.06	0.05	1.17	0.13	0.07	0.05
15	0.23	0.17	0.20	0.17	0.37	0.21	0.23	0.17

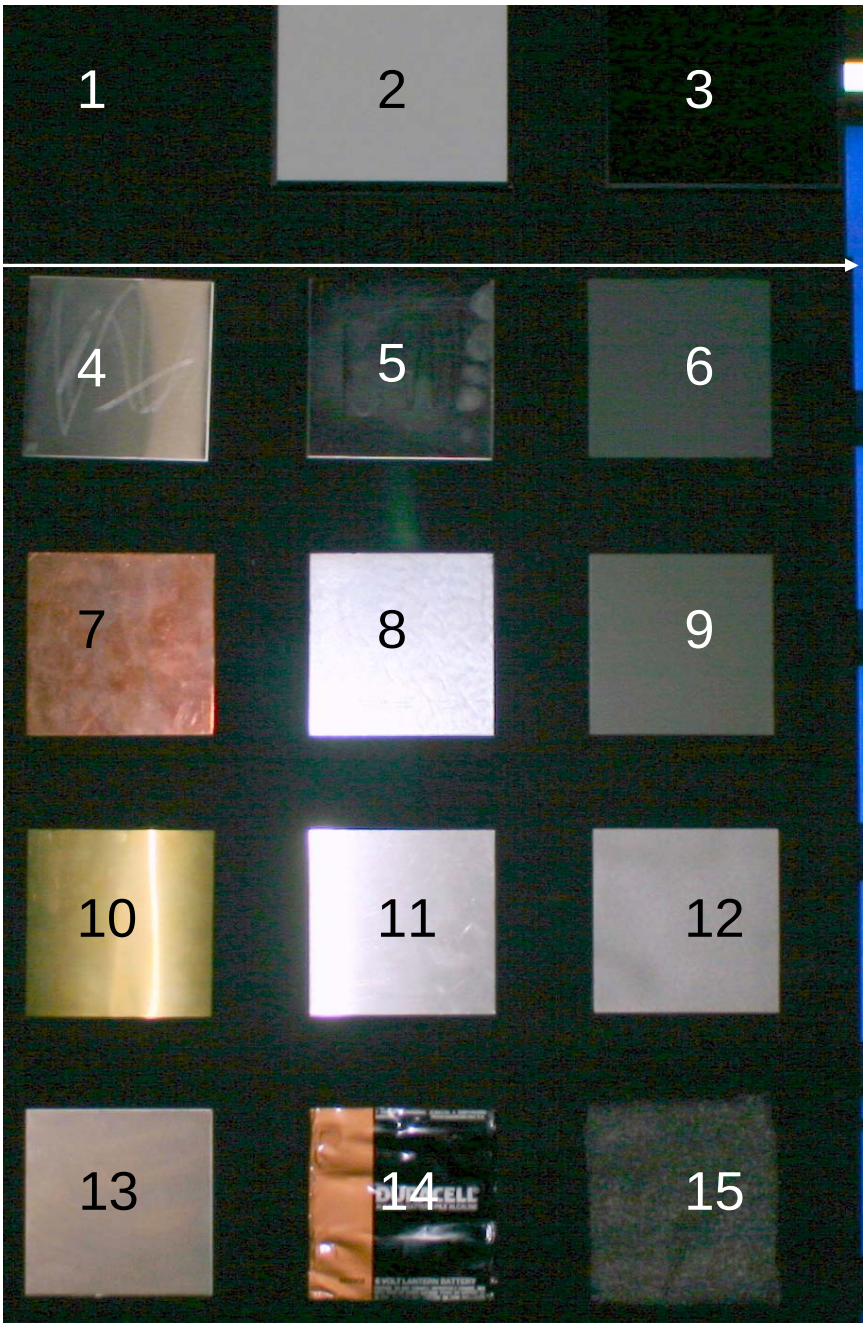

Figure 19: *Layout of metallic targets*

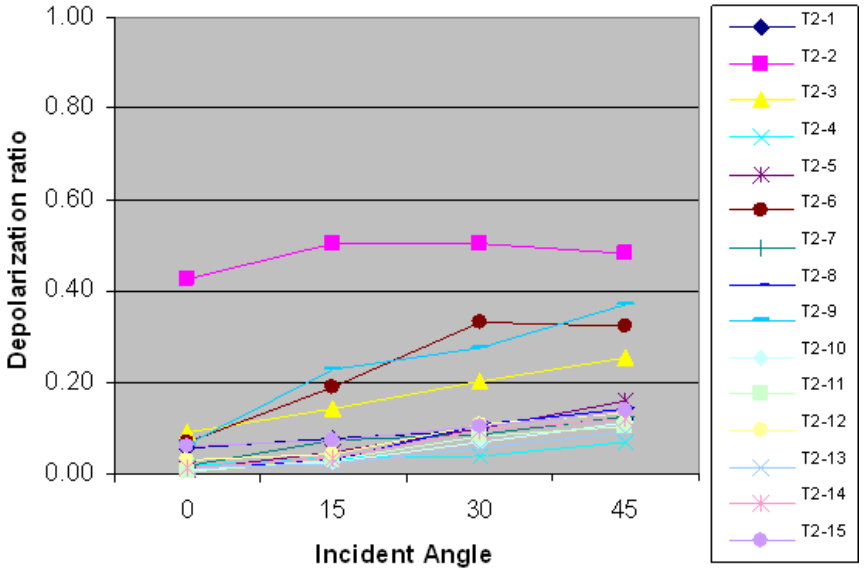

(a) Linear depolarization ratio (δ_L)

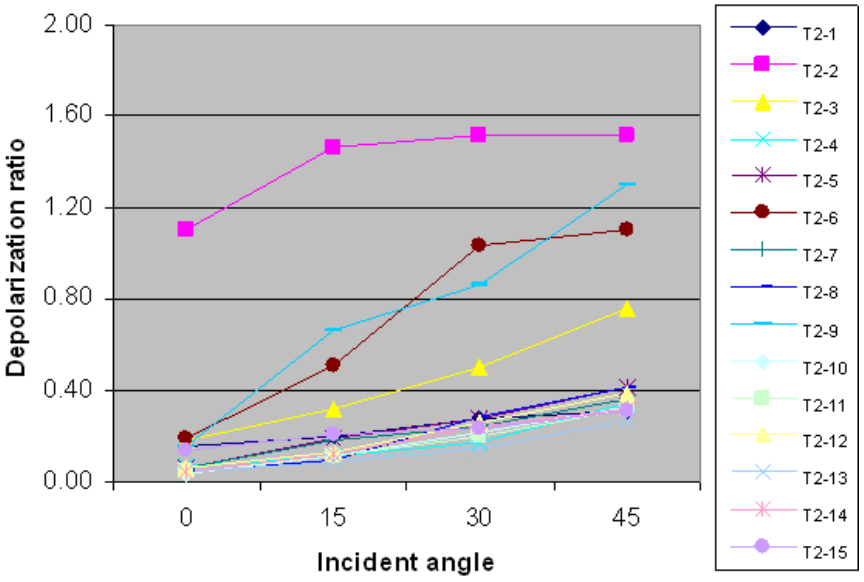

(b) Circular depolarization ratio (δ_C)

Figure 20: *Depolarization ratios of metallic targets and their changes with incident angle.*

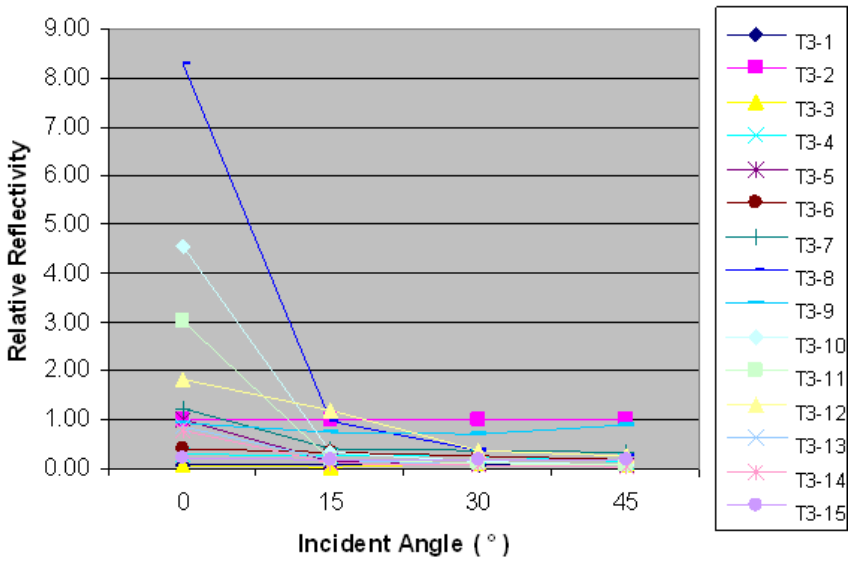

(a) Relative linear reflectivity

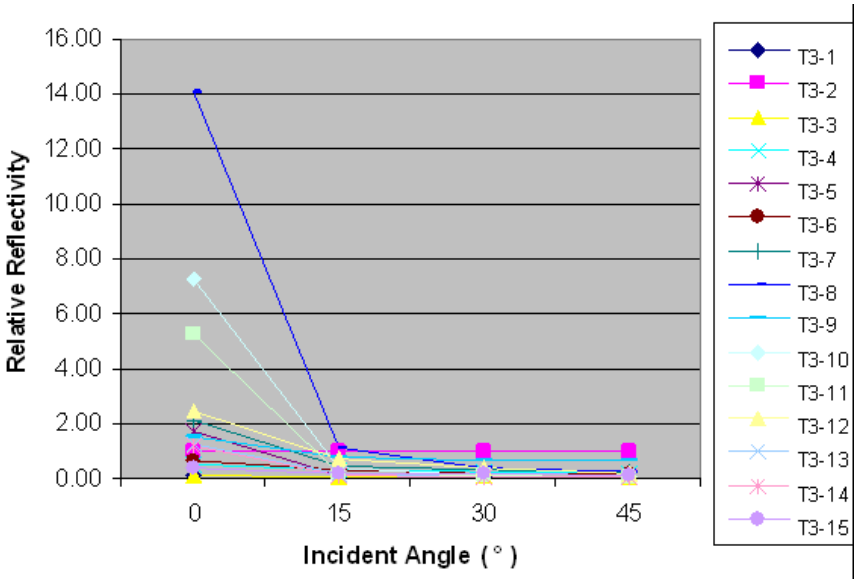

(b) Relative circular reflectivity

Figure 21: *Relative 21(a) linear reflectivities, and 21(b) circular reflectivity of metallic targets and their changes with incident angle*

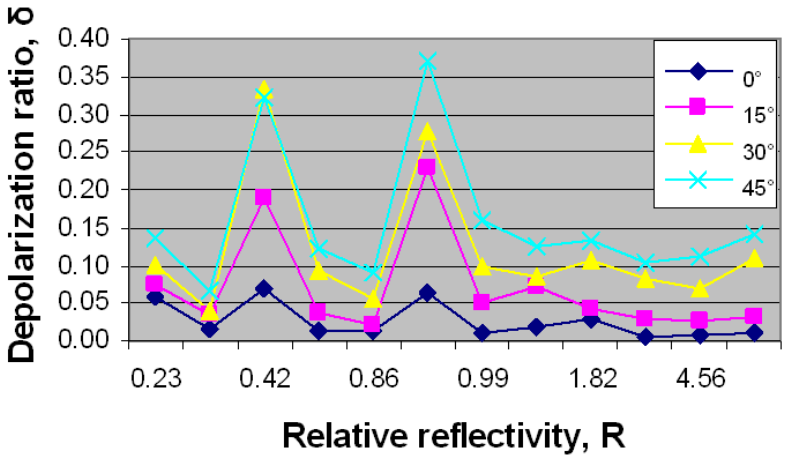

Figure 22: *Relationship between depolarization ratio and reflectivity of metallic targets*

4.4 Environmental targets

Environmental targets consist of cans and different pieces of plastic and glass bottles. Figure 23 shows some of these enviromental targets that were measured and Table 10 enumerates them.

Table 10: *Environmental targets and position of the center*

No	On the list	English Name	Center Position	
			x (cm)	y (cm)
1	Vide	Empty		
2	Spectralon blanc	White spectralon	25.4	6.75
3	Spectralon noir	Black Spectralon	44.45	6.75
4	Cannette de coke™écrasée	Crushed soda can	10	-6.5
5	Cannette de coke™ronde	Soda can	26	-6.5
6	Polyestère	Polyester	41	-6.5
7	Jute	Jute	10	-22
8	Cotton blanc	White cotton	26	-22
9	Chiffon J™	Chiffon	41.5	-22
10	Bouteille transparente ronde	Transp. plastic bottle	10	-37.5
11	Bouteille transparente écrasée	Crushed transp. plastic bottle	26	-37.5
12	Bouteille colorée	Colored plastic bottle	41.5	-37.5

The following subsections present the depolarization ratios and relative reflectivity analysis results following experiments conducted on these environmental targets.

4.4.1 Depolarization ratio

Depolarization ratio analysis is shown in Table 11 and corresponding trends are illustrated in Figure 24. Three groups can be formed based on the linear depolarization ratios. The first group {4, 5, 6} showed small depolarizations of value around 0.2. The second group {7, 9, 10, 11, 12} has depolairzations in the middle order, with value of about 0.4. The last group is target 8 (*cotton*) which showed the largest depolarization ratio among all the enviromental targets, whit value close to 0.6. The sequence changes a little when using circular depolarizations. In this situation, target 8 (*cotton*) and target 12 (*colored plastic bottle*) formed the third group.

Generally, the depolarization ratios of most enviromental targets slightly increased with incident angle from 0° to 30°, with the exception of target 5 (*soda can*) and target 10 (*transparent plastic bottle*). Both of them have curved surfaces and their depolarization ratio dramatically increased from 0° to 15°. Afterward, it decreased with greater rate when incident angle changed from 15° to 30°. Target 3 (*black Spectralon*) also showed sharp increase when incident angle increased to 45°. As this last result did not occured with the other panels, this result is unanticipated. A reason for this might be unexpected background signals due to a slight variation of the aerosols' density filling up the chamber during the measurements.

Table 11: *Depolarization ratio of enviromental targets*

Target #	Depolarization ratio							
	δ_L				δ_C			
	0 °	15 °	30 °	45 °	0 °	15 °	30 °	45 °
1	0.08	0.14	0.14	0.21	0.22	0.34	0.34	0.47
2	0.56	0.62	0.55	0.52	1.57	1.80	1.65	1.65
3	0.16	0.19	0.18	0.47	0.36	0.45	0.49	1.41
4	0.15	0.22	0.19	0.16	0.33	0.57	0.56	0.45
5	0.05	0.26	0.21	0.21	0.14	0.82	0.55	0.54
6	0.15	0.16	0.17	0.17	0.37	0.45	0.45	0.46
7	0.20	0.42	0.40	0.56	0.94	1.08	0.99	1.24
8	0.62	0.57	0.58	0.56	1.29	1.25	1.30	1.26
9	0.46	0.39	0.40	0.44	1.03	0.91	1.02	1.23
10	0.37	0.64	0.44	0.39	0.51	1.12	0.94	0.85
11	0.37	0.43	0.43	0.70	0.84	1.06	1.06	1.19
12	0.37	0.41	0.40	0.54	1.23	1.46	1.36	1.80
13	-	-	-	-	-	-	-	-
14	0.17	0.26	0.12	0.28	0.44	0.73	0.30	0.79

4.4.2 Relative reflectivity

Figure 25 illustrates the reflectivity of each environmental target and their change with the incident angle. Table 12 describes the analysis results of enviromental targets. Since it was difficult lo locate the position of the brown beer bottle based on the Andor image, this target was not included here.

Table 12: *Relative reflectivity results of enviromental targets*

Target #	Relative reflectivity							
	δ_L				δ_C			
	0 °	15 °	30 °	45 °	0 °	15 °	30 °	45 °
1	0.07	0.05	0.05	0.04	0.06	0.06	0.05	0.05
2	1.00	1.00	1.00	1.00	1.00	1.00	1.00	1.00
3	0.07	0.07	0.09	0.14	0.06	0.06	0.10	0.08
4	0.20	0.11	0.10	0.21	0.16	0.11	0.11	0.23
5	0.48	0.11	0.16	0.21	0.44	0.12	0.16	0.22
6	0.03	0.02	0.05	0.05	0.03	0.03	0.05	0.05
7	0.23	0.16	0.31	0.28	0.16	0.13	0.21	0.34
8	0.55	0.49	0.60	1.13	0.53	0.42	0.61	0.90
9	0.31	0.24	0.36	0.49	0.30	0.24	0.35	0.60
10	0.28	0.08	0.23	0.62	0.21	0.07	0.19	0.35
11	0.30	0.12	0.24	0.33	0.25	0.12	0.29	0.25
12	0.19	0.12	0.24	0.42	0.17	0.10	0.30	0.45
13	-	-	-	-	-	-	-	-
14	0.20	0.20	0.44	0.42	0.21	0.16	0.49	0.42

Figure 25 shows that reflectivity of enviromental targets dropped when incident angle changed from 0 ° to 15 °, then increased with the incident angle. Some initial

reflectivity drops are dramatical such as those for target 5 (*soda can*), target 10 (*transparent plastic bottle*), and target 11 (*crushed transparent plastic bottle*). From 15 ° to 45 ° , the reflectivity linearly increased approximately with the incident angle for most enviromental targets.

Without surprise, target 6 (*polyester*) showed smallest reflectivity because of its dark color. Target 4 (*crushed can*) and target 11 (*crushed transparent plastic bottles*) showed comparative reflectivities to their corresponding normal ones (i.e. target 5 and target 10). Target 8 (*white cotton*) showed much higher reflectivity that other targets on the same panel. Moreover, at 45 ° incident angle, target 8 showed comparative reflectivity to target 2 (*white Spectralon*). This is surely due to its white color.

The result analysis also demonstrated that white targets showed reflectivity among the highest. Consequently, targets with dark colors showed reflectivity among the lowest.

Target 8 (*cotton*) showed the highest reflectivity and the largest depolarization ratio. Targets 4 (*crushed soda can*), 5 (*soda can*), and 6 (*polyester*) showed relatively low reflectivity, and their depolarization ratios are in the smallest depolarization group. Consequently, a conclusion can be drawn wrt to the fact that the depolarization ratio increased genenally with the reflectivity of the environemental targets (as shown in Figure 26). This also implied that the depolarization ratio is function of the reflectivity of the target, as well as of other target properties (e.g. surface roughness, etc.).

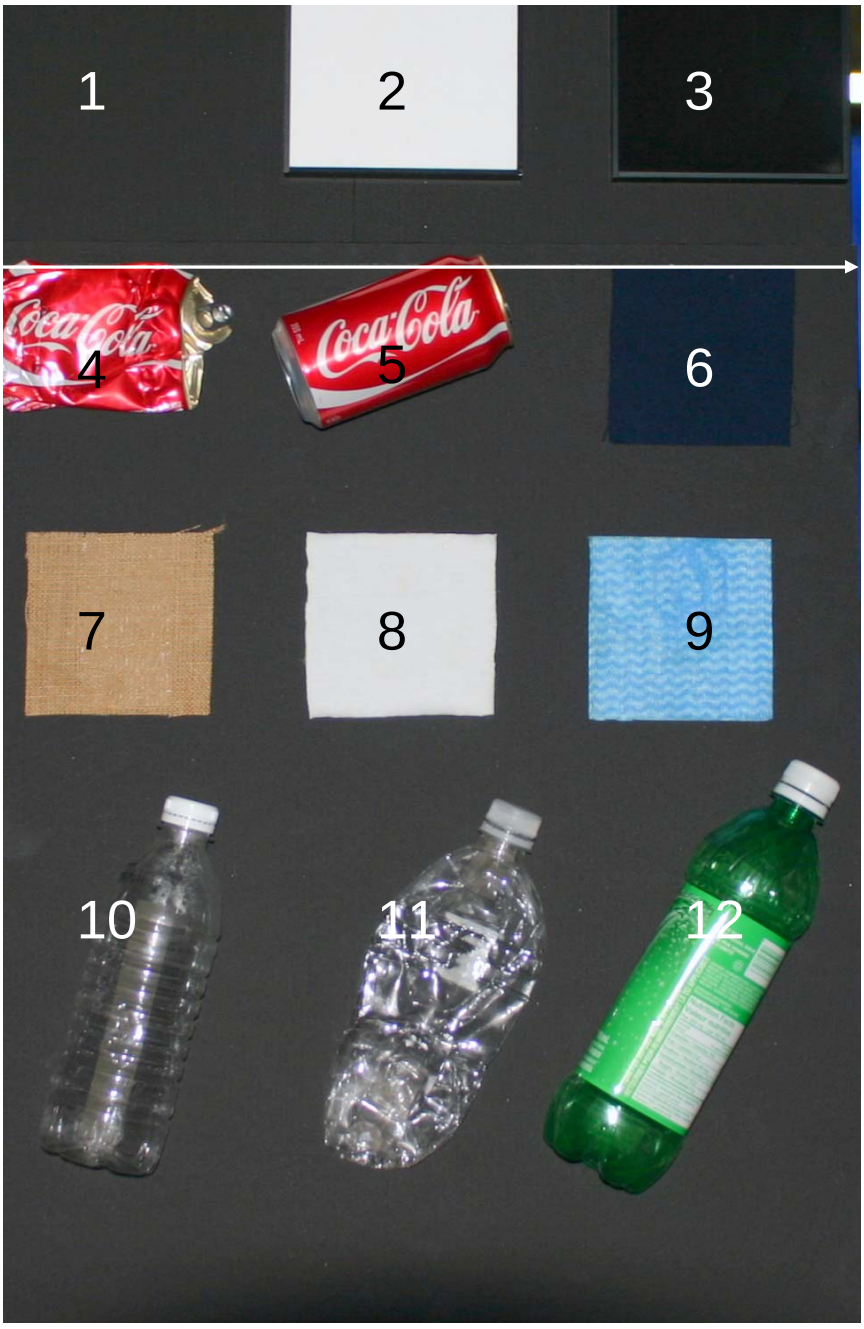

Figure 23: *Layout of environmental targets*

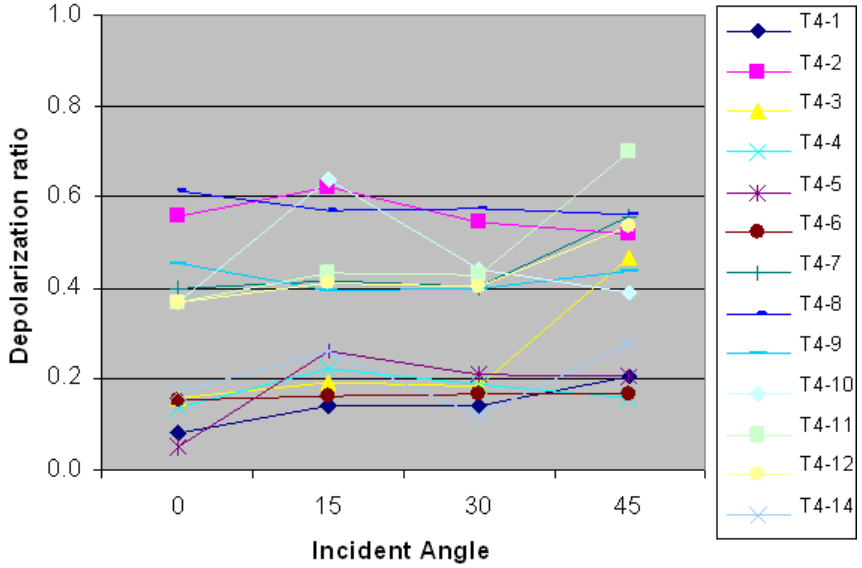

(a) Linear depolarization ratio (δ_L)

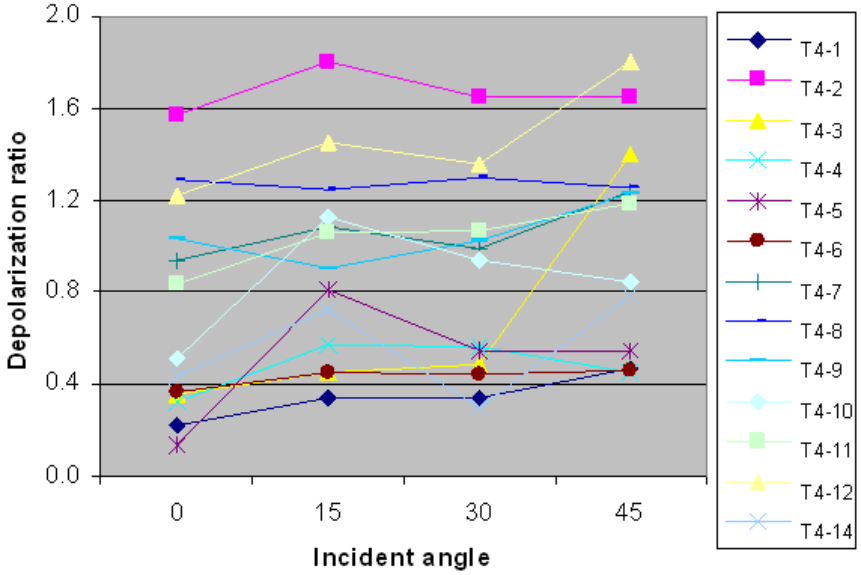

(b) Circular depolarization ratio (δ_C)

Figure 24: *Depolarization ratios of enviromental targets and their changes with incident angle.*

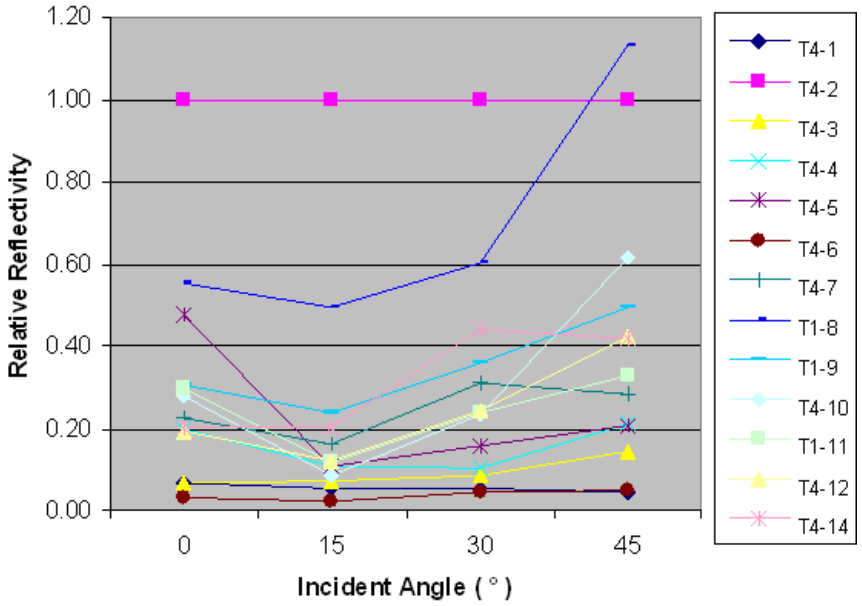

(a) Relative linear reflectivity

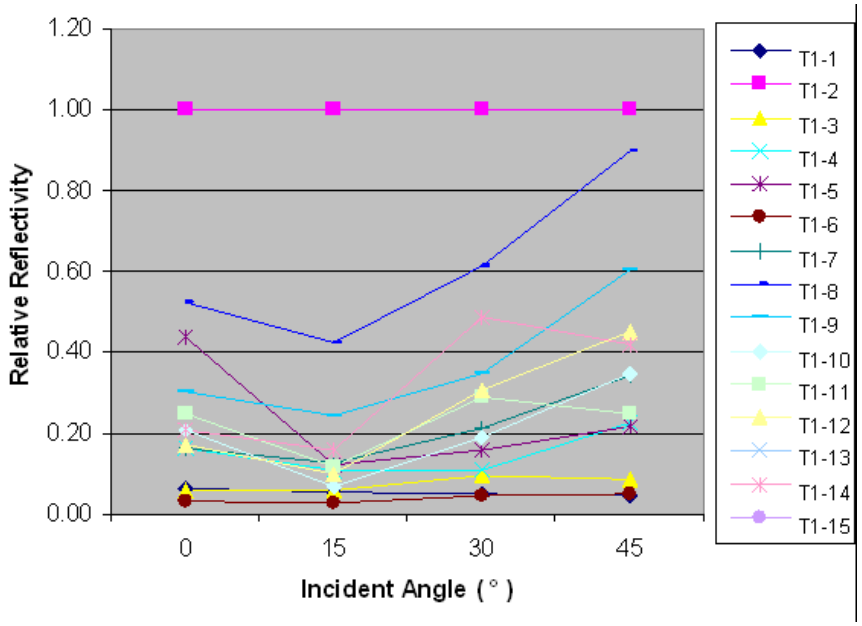

(b) Relative circular reflectivity

Figure 25: *Relative 25(a) linear reflectivity, and 25(b) circular reflectivity of enviromental targets and their changes with incident angle*

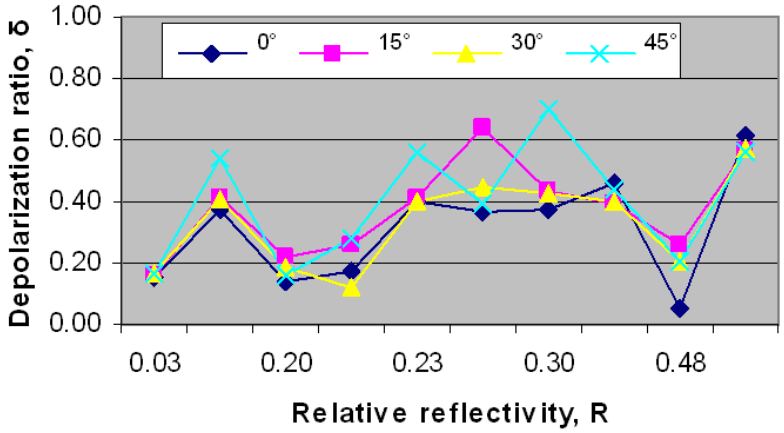

Figure 26: *Relationship between depolarization ratio and reflectivity of environmental targets*

4.5 Sand paper targets

Different grit sand papers and some other material targets were glued on Panel 5 and examined together. The description for these targets can be found in Table 13 and they are illustrated in Figure 28.

Table 13: *Sand papers and position of the center*

No	On the list	English Name	Center Position	
			x (cm)	y (cm)
1	Vide	Empty		
2	Spectralon blanc	White Spectralon	25.4	6.75
3	Spectralon noir	Black Spectralon	44.45	6.75
4	Papier sablé 50	Sand paper 50	10	-6.5
5	Papier sablé 100	Sand paper 100	26	-6.5
6	Papier sablé 220	Sand paper 220	41	-6.5
7	Papier sablé 400	Sand paper 400	10	-22
8	Papier sablé 600	Sand paper 600	26	-22
9	Papier sablé 1000	Sand paper 1000	41.5	-22
10	Papier sablé 1500	Sand paper 1500	10	-37.5
11	Sac de papier	Paper bag	26	-37.5
12	Carton	Carton	41.5	-37.5
13	Sac de plastique transparent	Transparent plastic bag	9.4	-54.5
14	Sac de plastique Métro™blanc	White plastic bag	26.5	-52

The following subsections present the depolarization ratios and relative reflectivity analysis results following experiments conducted on these sand paper targets.

4.5.1 Depolarization ratios

The depolarization ratios of the sand paper targets on panel 5 are shown in Table 14, and corresponding plots are illustrated in Figure 27. Target 14 (*white plastic bag*) showed the largest linear depolarization ratio among all targets on panel 5, while target 7 (*sand paper 400*) showed the smallest one (close to target 3 which is the *black Spectralon*). The targets sequence in decrease order, based on the depolarization ratio, is: $\delta_{14} \geq \delta_6 \geq \delta_5 > \delta_4 > \delta_{11} > \delta_{12} \geq \delta_8 > \delta_{10} \geq \delta_9 > \delta_7$. Typically, for targets of the same colors (e.g. targets 7, 9, and 10), the depolarisation ratio increases with the number grits. Target 13 (*transparent plastic bag*) is a very special one: its linear depolarization ratio started from the smallest at incident angle 0°, and quickly jumped to the group of light color sand papers. The circular depolarization ratio of target 13 only increased from incident angle 0° to 15°, then decreased when incident angle further increased. This may be due to the uneven surface of target 13, and that multi-scaterring was actually in effect. The target sequence of panel 5, based on the circular depolarization ratio, is slightly different from the linear ones. Generally, all target depolarization ratios increased linearly with the incident angle with approximately (with some exceptions) the circular depolarization ones from

30 ° to 45 ° . Circular depolarization ratios are usually 2.5 ∽ 3 times of linear ones, with exception of target 13 which showed much higher ratios.

Table 14: *Depolarization ratio of sand paper targets*

Target #	Depolarization ratio							
	δ_L				δ_C			
	0 °	15 °	30 °	45 °	0 °	15 °	30 °	45 °
1	0.07	0.10	0.14	0.16	0.26	0.32	0.36	0.42
2	0.45	0.51	0.52	0.60	1.32	1.52	1.56	1.42
3	0.13	0.24	0.28	0.28	0.57	0.67	0.72	0.57
4	0.36	0.41	0.46	0.46	0.98	1.14	1.40	1.21
5	0.46	0.48	0.48	0.49	1.32	1.48	1.50	1.32
6	0.49	0.46	0.53	0.50	1.24	1.24	1.48	1.30
7	0.13	0.14	0.15	0.19	0.32	0.35	0.40	0.57
8	0.27	0.32	0.35	0.39	0.74	0.90	1.05	0.75
9	0.16	0.18	0.24	0.28	0.39	0.46	0.66	0.74
10	0.22	0.25	0.29	0.30	0.67	0.73	0.85	0.80
11	0.31	0.39	0.41	0.43	1.03	1.25	1.42	1.29
12	0.30	0.34	0.40	0.39	0.90	1.08	1.35	1.35
13	0.07	0.20	0.35	0.46	0.96	1.39	1.14	0.93
14	0.43	0.57	0.57	0.60	0.91	1.25	1.25	1.43

4.5.2 Relative reflectivity

The reflectivity and relationship with the incident angle is shown in Figure 29. Analysis results is shown in Table 15.

All targets reflectivity decreased with incident angle from 0 ° to 30 ° , and then slightly increased or remained unchanged from incident angle 30 ° to 45 ° .

Target 13 (*transparent plastic bag*) shown the largest reflectivity initially (at angle 0 °), then dropped dramatically to a small value in both situations of linear and circular polarized lights. This might results from the multi-scattering due to uneven surface of the target. The decreased order of sand paper targets based on their reflectivity is: 6 → 5 → 4 → 8 → 14 → 12 → 11 → 9 → 13 → 7 → 10. Target 4 (*sand paper 50*) to target 10 (*sand paper 1500*) are sand papers with increasing grit number, where targets 4 (*sand paper 50*), 5 (*sand paper 100*), and 6 (*sand paper 220*) are in light colors. Targets 7 (*sand paper 400*), 9 (*sand paper 1000*), and 10 (*sand paper 1500*) are in dark colors. Target 8 (*sand paper 600*) has a neutral color between black and white. Obviously, for sand papers, the lighter the color and the finer the sand grit, the stronger the reflectivity and vice versa. Target 10 (*sand paper 1500*) is an exception with the smallest sand grit but the weaker reflectivity.

Figure 30 illustrates a clear trend that depolarization ratio of sand papers and some other targets on this panel increased with the target reflectivity. The depolarization

Table 15: *Relative reflectivity results of sand paper targets*

Target #	Relative reflectivity							
	δ_L				δ_C			
	0 °	15 °	30 °	45 °	0 °	15 °	30 °	45 °
1	0.10	0.07	0.06	0.06	0.11	0.09	0.06	0.07
2	1.00	1.00	1.00	1.00	1.00	1.00	1.00	1.00
3	0.14	0.10	0.08	0.08	0.12	0.10	0.08	0.08
4	0.73	0.56	0.42	0.46	0.75	0.62	0.44	0.46
5	0.73	0.71	0.52	0.61	0.79	0.82	0.52	0.59
6	1.00	0.99	0.61	0.66	1.01	0.91	0.61	0.61
7	0.16	0.13	0.08	0.09	0.22	0.18	0.08	0.10
8	0.60	0.50	0.31	0.30	0.64	0.56	0.29	0.28
9	0.27	0.19	0.11	0.12	0.28	0.23	0.11	0.11
10	0.09	0.06	0.07	0.09	0.09	0.07	0.09	0.11
11	0.26	0.22	0.21	0.18	0.32	0.24	0.22	0.19
12	0.28	0.24	0.20	0.23	0.26	0.24	0.20	0.24
13	1.04	0.13	0.10	0.12	1.35	0.16	0.11	0.11
14	0.42	0.34	0.38	0.42	0.43	0.32	0.33	0.40

ratio increased with the incident angle too, but the decrease rate after 15 ° was small. For targets on this panel, it seems that a linear relationship between depolarization ratio and incident angle can be drawn.

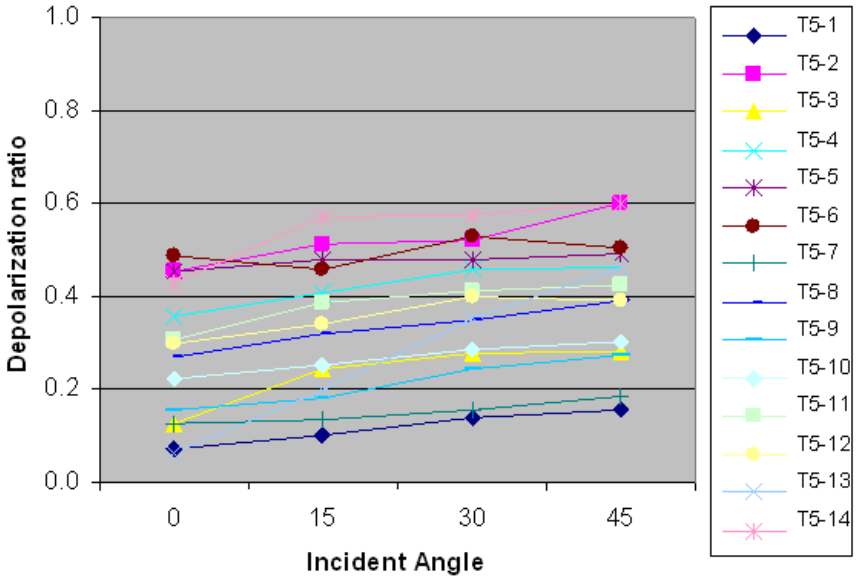

(a) Linear depolarization ratio (δ_L)

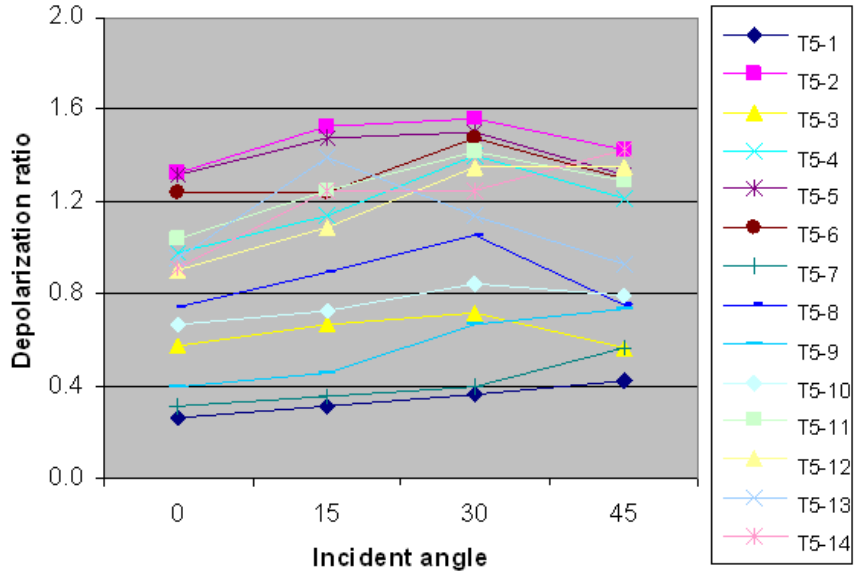

(b) Circular depolarization ratio (δ_C)

Figure 27: *Depolarization ratios of sand papers targets and their changes with incident angle.*

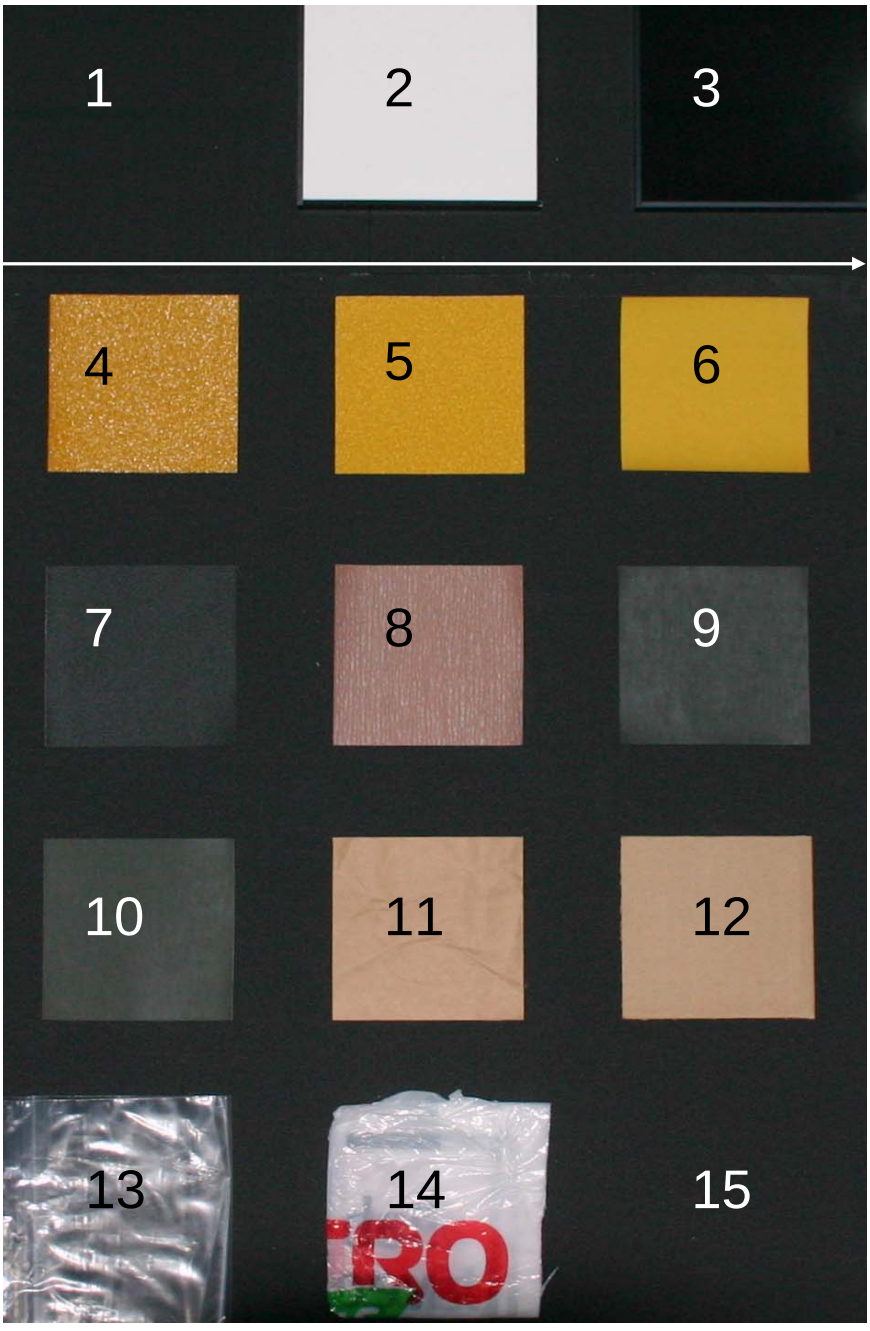

Figure 28: *Layout of sand paper targets*

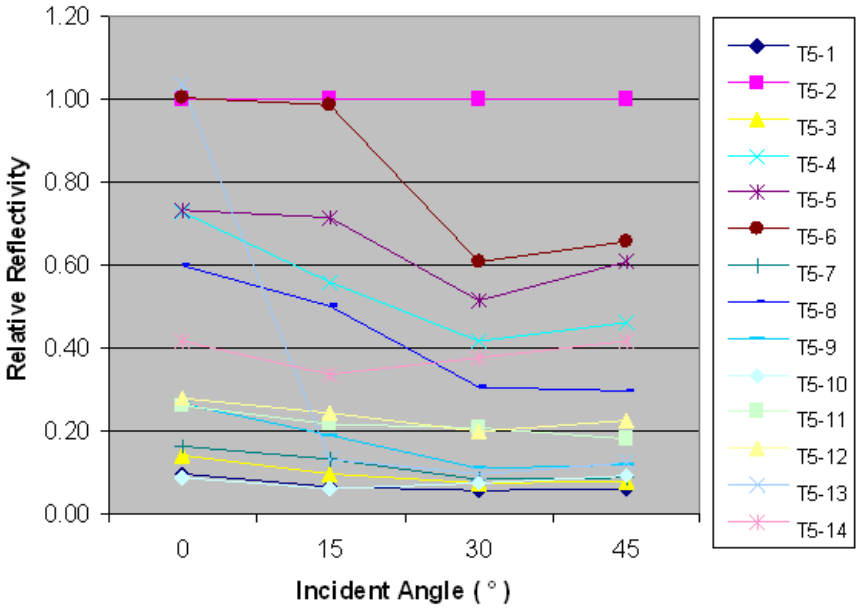

(a) Relative linear reflectivity

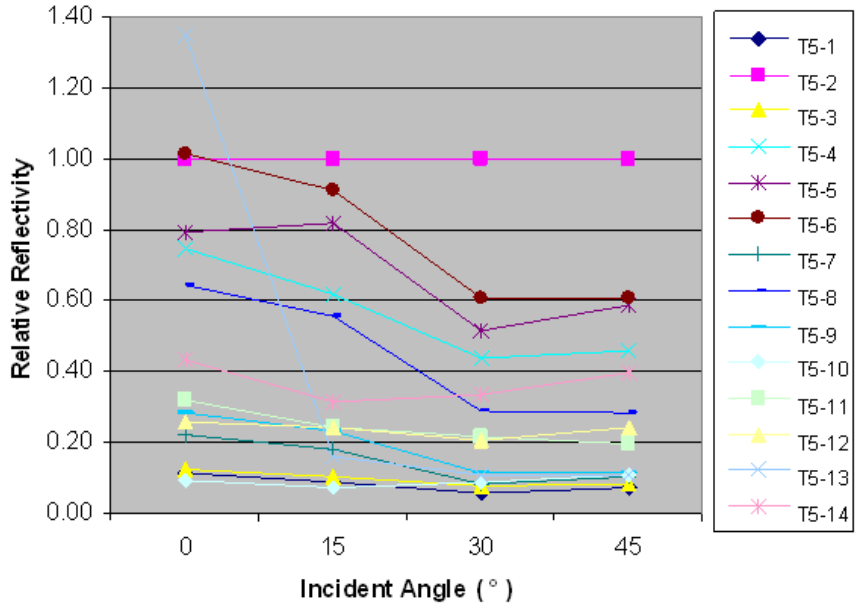

(b) Relative circular reflectivity

Figure 29: *Relative 29(a) linear reflectivity, and 29(b) circular reflectivity of sand papers targets and their changes with incident angle*

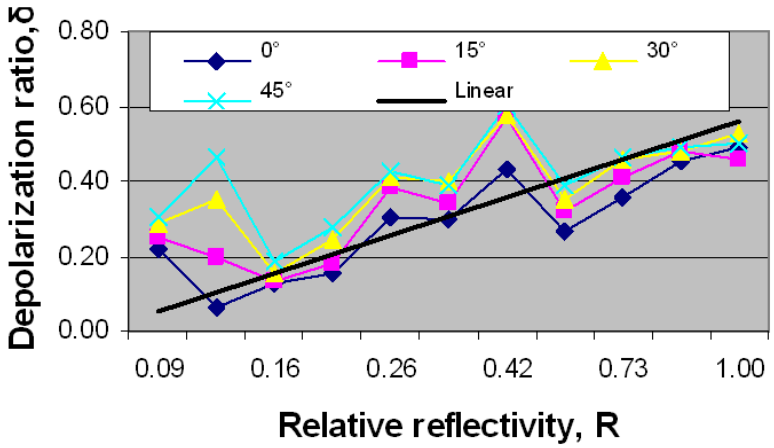

Figure 30: *Relationship between depolarization ratio and reflectivity of sand paper targets*

4.6 Composite plastic targets

Composite plastic targets on panel 6 are shown in Figure 31 and described in Table 16.

Table 16: *Composite plastic targets and position of the center*

No	On the list	English Name	Center Position	
			x (cm)	y (cm)
1	Vide	Empty		
2	Spectralon blanc	White Spectralon	25.4	6.75
3	Spectralon noir	Black Spectralon	44.45	6.75
4	Caoutchouc noir	Black rubber	10	-6.5
5	Silicone orange	Orange silicone	26	-6.5
6	Teflon™(polytetrafluoroethylene)	Polytetrafluoroethylene (Teflon™)	41	-6.5
7	Acrylique + PVC Kydex 100	Flame retardant sheet (Kydex Acrylic PVC)	10	-22
8	Poly-Éthylène-Haute-Densité	High density polyethylene	26	-22
9	NEMA Phénolique + Fibre de verre	Nema phenolic (glass fiber reinforced)	41.5	-22
10	Acétal Delrin™	Acetal (Delrin™)	10	-37.5
11	Styrène Opaque	Opaque styrene	26	-37.5
12	Vinyle couleur sable	Sand-color vinyl	41.5	-37.5
13	Vitre de plastique	Plastic glass	10	-54.5
14	Lexan™	Polycarbonate resin thermoplastic (Lexan™)	26	-54.5
15	Bâche	Tarpaulin	41.5	-54.5

The following subsections present the depolarization ratios and relative reflectivity analysis results following measurements conducted on these composite plastic targets.

4.6.1 Relative reflectivity

Results of reflectivity examination of each target is shown in Table 17. Figure 32 illustrates the corresponding chart of relative reflectivity of each target on panel 6 and their change with the incident angle. It is found that reflectivity of most composite plastic targets slighlty decreased with incident angle with the exception of targets 10 (*acetal*), 11 *opaque styrene*, and 12 (*sand-color vinyl*) which increased a little at least from 0° to 15°. For most targets, the major change happened when incident angle varied from 0° to 15°. In that case, target 9 (*nema phenolic*) showed the largest change similar to some metallic targets. For other targets, the change mainly happened from 0° to 15°, where the reflectivity remained almost unchanged. This is the case for targets 4 (*black rubber*), 5 (*orange silicone*), 6 (*polytetrafluoroethylene*), 9 (*nema phenolic*). The incident angle seems to have little influence on a few targets such as target 7 (*flame retardant sheet*) and target 8 (*high density polyethylene*). Of all composite plastic targets, those with light colors (i.e. targets 6, 8, 10, 11, 12,

15) showed larger reflectivities than those with dark colors (targets 4, 5, 9, 13, 14). Subsequently, the black ones showed least reflectivity.

Table 17: *Relative reflectivity results of composite plactic targets*

Target #	Relative reflectivity							
	δ_L				δ_C			
	0 °	15 °	30 °	45 °	0 °	15 °	30 °	45 °
1	0.06	0.07	0.05	0.05	0.07	0.08	0.05	0.05
2	1.00	1.00	1.00	1.00	1.00	1.00	1.00	1.00
3	0.08	0.08	0.09	0.08	0.08	0.08	0.07	0.06
4	0.20	0.07	0.05	0.05	0.23	0.07	0.04	0.05
5	0.28	0.12	0.09	0.10	0.31	0.12	0.07	0.09
6	1.38	1.07	1.02	1.05	1.17	0.87	0.73	0.87
7	0.31	0.33	0.27	0.29	0.31	0.31	0.20	0.22
8	0.72	0.71	0.70	0.69	0.60	0.56	0.42	0.58
9	1.93	0.14	0.12	0.12	2.15	0.13	0.08	0.10
10	0.46	0.84	0.74	0.68	0.39	0.68	0.49	0.50
11	0.93	0.96	1.34	1.05	0.90	1.02	1.11	1.26
12	0.57	0.86	1.03	0.84	0.49	0.82	0.77	0.63
13	0.19	0.12	0.08	0.08	0.21	0.12	0.06	0.08
14	0.18	0.12	0.11	0.10	0.16	0.12	0.09	0.09
15	0.73	0.52	0.36	0.29	0.85	0.62	0.33	0.33

4.6.2 Depolarization ratios

Depolarization ratios of composite plastic targets on panel 6 and their change is shown in Table 18 and illustrated in Figure 33. Like most other panel targets, depolarization ratios of most composite plastic targets increased with the incident angle, with exception of target 14 (*plastic glass*) which depolarization ratio decreased when the incident angle was greater than 15 °. Based on previous observations of other panel targets, composite plastic targets with light colors (also great reflectivity) showed larger depolarization ratios (i.e. targets 6, 8, 10, 11, and 12). Targets with dark colors (less reflectivity) showed smaller depolarization ratios (i.e. targets 4, 5, and 9) when considering their corresponding reflectivity. The surprising result is target 14 which had the smallest reflectivity but showed almost largest depolarization ratio among those targets on the same panel (Figure 34).

Table 18: *Depolarization ratio of composite plastic targets*

Target #	Depolarization ratio							
	δ_L				δ_C			
	0 °	15 °	30 °	45 °	0 °	15 °	30 °	45 °
1	0.10	0.11	0.13	0.16	0.28	0.32	0.39	0.45
2	0.46	0.48	0.50	0.47	1.27	1.45	1.53	1.52
3	0.24	0.29	0.36	0.35	0.46	0.64	0.86	0.77
4	0.05	0.14	0.21	0.25	0.09	0.33	0.55	0.64
5	0.08	0.22	0.31	0.32	0.16	0.53	0.76	0.89
6	0.52	0.71	0.74	0.81	0.70	1.00	1.08	1.26
7	0.18	0.24	0.36	0.37	0.45	0.73	1.05	1.31
8	0.53	0.83	0.74	0.77	0.66	1.00	0.86	1.02
9	0.03	0.34	0.41	0.41	0.06	0.92	1.27	1.25
10	0.42	0.75	0.83	0.84	0.49	0.88	1.00	1.10
11	0.26	0.55	0.51	0.53	0.60	1.57	1.53	1.81
12	0.28	0.42	0.44	0.43	0.90	1.49	1.63	1.65
13	0.06	0.13	0.20	0.28	0.10	0.30	0.46	0.73
14	0.80	0.98	0.80	0.67	1.30	1.84	1.66	1.54
15	0.14	0.20	0.35	0.43	0.75	0.91	1.05	1.16

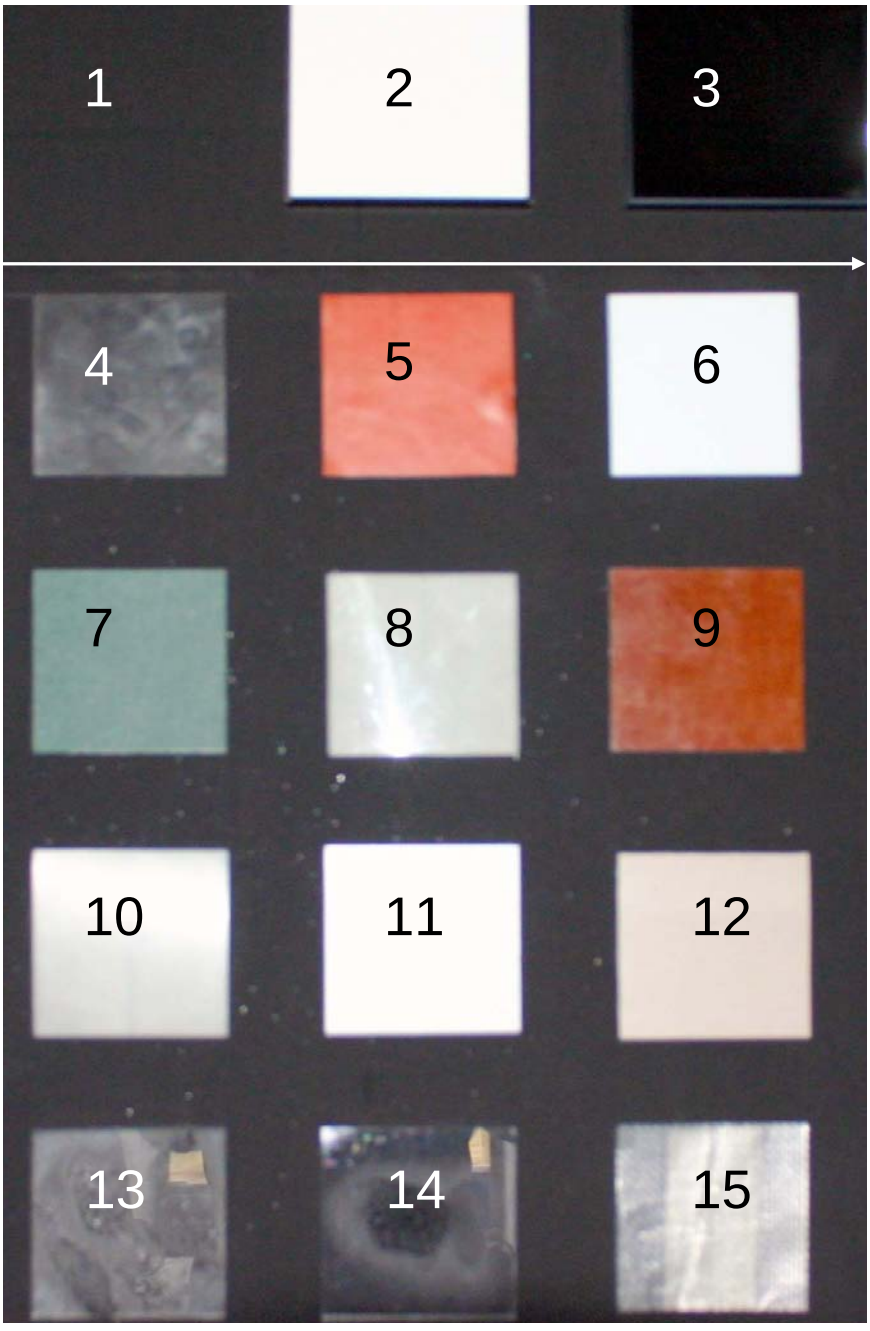

Figure 31: *Layout of composite plastic targets*

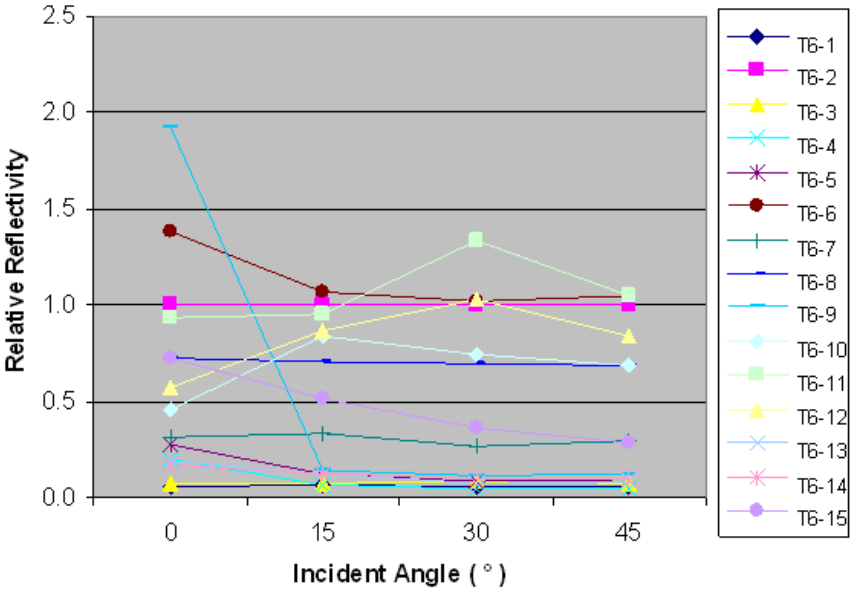

(a) Relative linear reflectivity

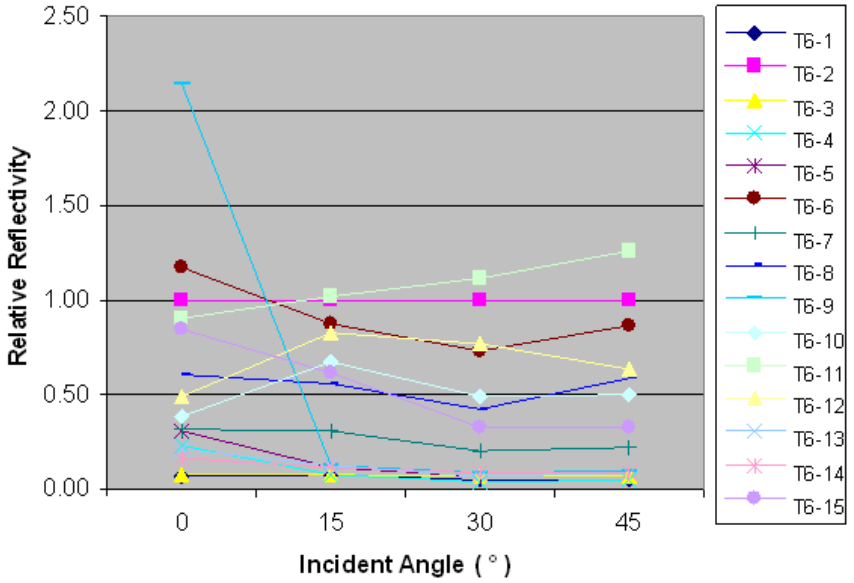

(b) Relative circular reflectivity

Figure 32: *Relative 32(a) linear reflectivities, and 32(b) circular reflectivity of composite plastic targets and their changes with incident angle.*

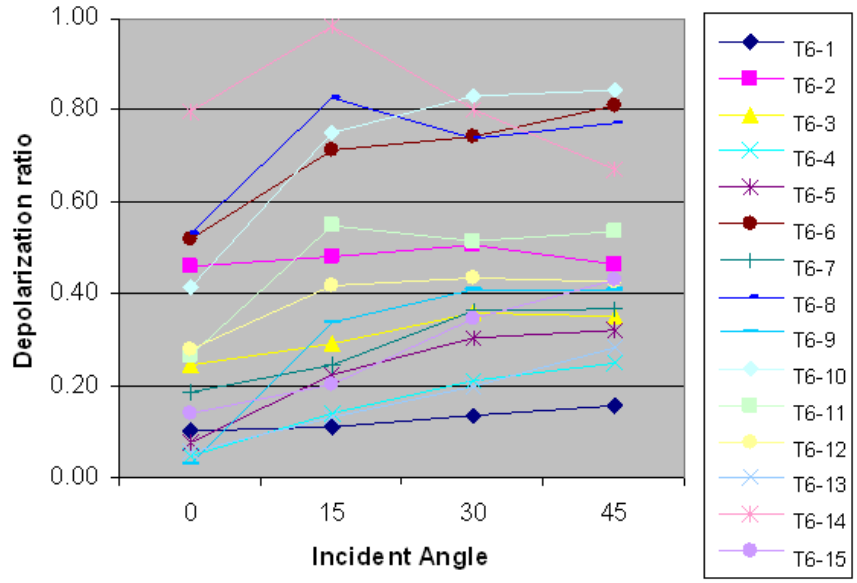

(a) Linear depolarization ratio (δ_L)

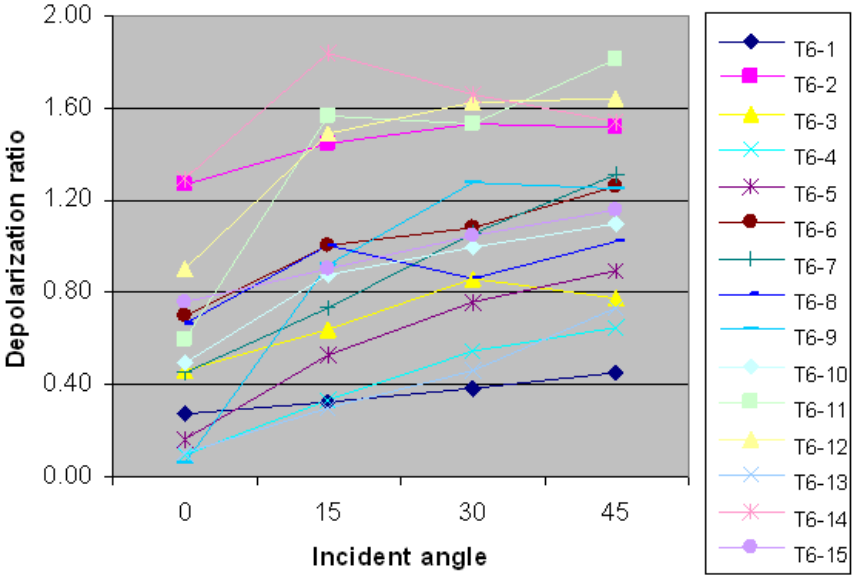

(b) Circular depolarization ratio (δ_C)

Figure 33: *Depolarization ratios of composite plastic targets and their changes with incident angle.*

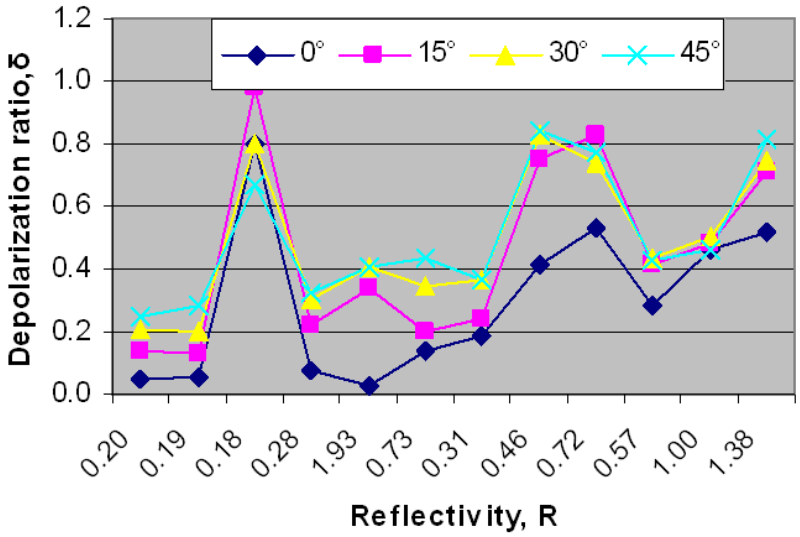

Figure 34: *Relationship between depolarization ratio and reflectivity of composite plastic targets.*

4.7 Sands

Both dry and wet fine (white) and coarse (dark) sands were examined. These targets are presented on Table 19 and illustrated in Figure 35.

Table 19: *Sand types and position of the center*

No	On the list	English Name	Center Position	
			x (cm)	y (cm)
1	Vide	Empty		
2	Spectralon blanc	White Spectralon	25.4	6.75
3	Spectralon noir	Black Spectralon	44.45	6.75
4	Sable mouillé/sec 000	Wet/dry sand 000	11.65	-25.5
5	Sable mouillé/sec 030	Wet/dry sand 030	42.15	-25.5

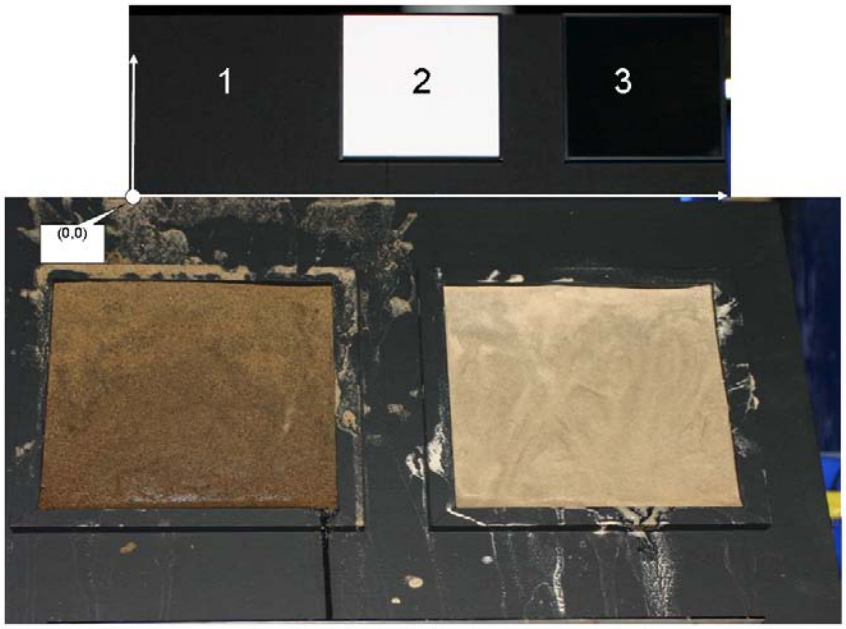

Figure 35: *Layout of sand targets*

The following subsections present the depolarization ratios and relative reflectivity analysis results following experiments conducted on these sand targets.

4.7.1 Relative reflectivity

The analysis results of relative reflectivity is shown in Table 20 and Figure 36.

Figure 36 shows that target 3 (*dry fine sand*) had largest reflectivity and target 4 (*wet coarse sand*) showed less reflectivity. Coarse sands always showed less reflectivity than fine sands no matter dry or wet. Subsequently, wet sands, fine or coarse, always showed smaller reflectivity than dry ones. Reflectivity of dry sands, no matter fine

Table 20: *Relative reflectivity results of sands*

Target #	Relative reflectivity							
	δ_L				δ_C			
	0 °	15 °	30 °	45 °	0 °	15 °	30 °	45 °
1	1.00	1.00	1.00	1.00	1.00	1.00	1.00	1.00
2	0.49	0.45	0.70	0.70	0.52	0.44	0.63	0.65
3	0.79	0.80	0.99	0.89	0.77	0.73	0.90	0.90
4	0.15	0.14	0.13	0.19	0.14	0.13	0.13	0.20
5	0.52	0.38	0.34	0.62	0.38	0.35	0.29	0.54

or coarse, increased with incident angle, while wet sands decreased from 0 ° to 30 ° or hardly changed.

4.7.2 Depolarization ratios

Analysis results of depolarization ratios is shown in Table 21 and illustrated in Figure 37. Depolarization ratio of sands hardly changed with incident angle from 0 ° to 30 °. They showed noticeable alteration when incident angle changed from 0 ° to 45 °. However, there was little change of the depolarization ratios of the dry sands. Similar to reflectivity, fine sands showed higher depolarization ratios than coarse sands, no matter dry or wet. Furthermore, depolarization ratio of wet fine sands was greater than dry fine sands, but not so much difference between wet and dry coarse sands except at incident angle of 45 °. Circular depolarization ratios of sands are $2 \sim 2.5$ times the values of linear ones.

Table 21: *Depolarization ratio of sands*

Target #	Depolarization ratio							
	δ_L				δ_C			
	0 °	15 °	30 °	45 °	0 °	15 °	30 °	45 °
1	0.48	0.51	0.54	0.48	1.41	1.51	1.63	1.61
2	0.45	0.46	0.43	0.44	1.24	1.20	1.19	1.23
3	0.55	0.56	0.57	0.53	1.21	1.23	1.28	1.22
4	0.42	0.41	0.42	0.59	0.83	0.82	0.88	1.02
5	0.68	0.65	0.65	0.80	1.09	1.07	1.11	1.17

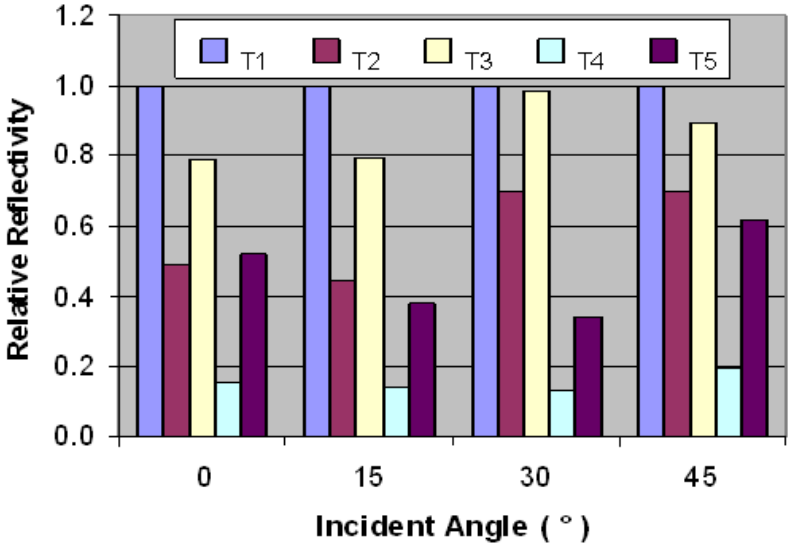

(a) Relative linear reflectivity

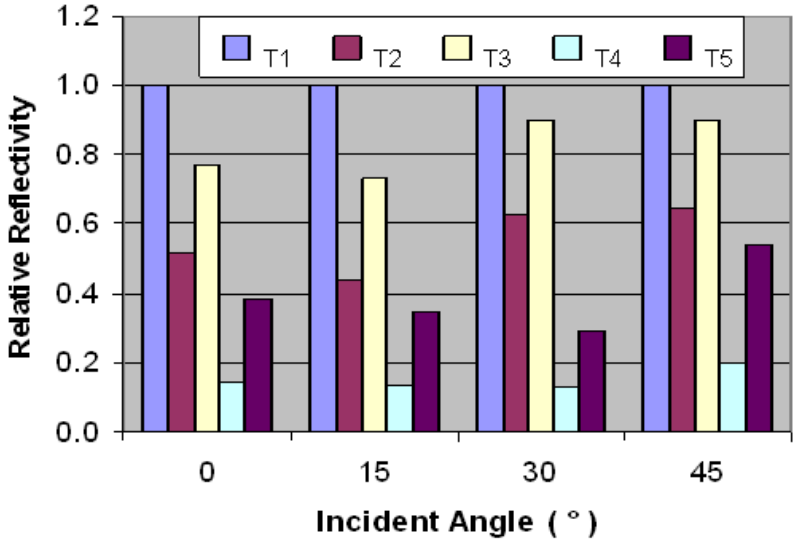

(b) Relative circular reflectivity

Figure 36: *Relative 36(a) linear reflectivities, and 36(b) circular reflectivity of sands and their changes with incident angle.*

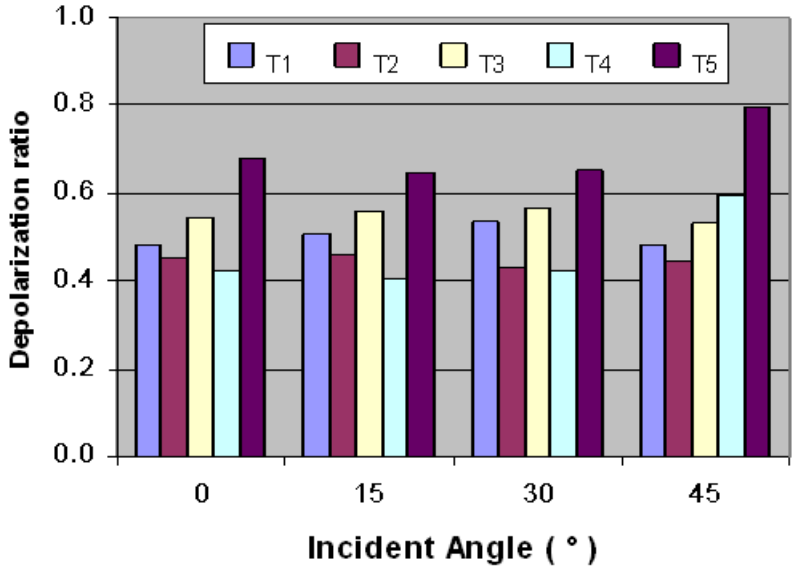

(a) Linear depolarization ratio (δ_L)

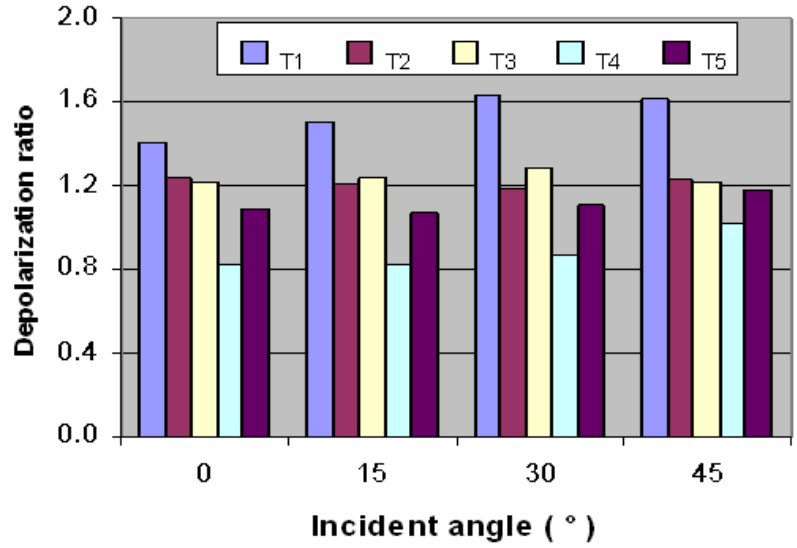

(b) Circular depolarization ratio (δ_C)

Figure 37: *Depolarization ratios of sands and their changes with incident angle.*

4.8 Construction materials and grass

Concrete, asphalt, and two different fresh grass packets were examined. Figures 38 and 39 illustrate the grass and construction targets, respectively. As with previous panels, white Spectralon is included in the panel to get the relative reflectivity of each target.

Figure 38: *Layout of grass targets*

The reflectivity and depolarization ratios for construction targets and grass are presented in Table 22 and Table 23, respectively.

Table 22: *Relative reflectivity results of construction and grass targets*

Target #	Relative reflectivity							
	δ_L				δ_C			
	0 °	15 °	30 °	45 °	0 °	15 °	30 °	45 °
1	1.00	1.00	1.00	1.00	1.00	1.00	1.00	1.00
2	0.41	0.42	0.43	0.53	0.46	0.41	0.42	0.51
3	0.20	0.14	0.18	0.22	0.20	0.15	0.18	0.23
4	0.18	0.09	0.08	0.13	0.13	0.09	0.09	0.11
5	0.62	0.35	0.35	0.55	0.54	0.36	0.37	0.46

Figure 40 and Figure 41 illustrate corresponding charts of the reflectivity and depolarization ratio and their change with incident angle of light.

Figure 39: *Layout of concrete and asphalt targets*

Table 23: *Depolarization ratio of construction and grass targets*

Target #	Depolarization ratio							
	δ_L				δ_C			
	0 °	15 °	30 °	45 °	0 °	15 °	30 °	45 °
1	0.48	0.53	0.50	0.47	1.45	1.54	1.63	1.58
2	0.38	0.41	0.35	0.39	1.24	1.28	1.12	1.26
3	0.30	0.37	0.36	0.36	0.85	1.06	1.13	1.09
4	0.20	0.27	0.28	0.26	0.47	0.63	0.70	0.66
5	0.41	0.37	0.37	0.37	1.05	0.98	1.01	1.00

4.8.1 Relative reflectivity

Reflectivity of these targets has little change with the incident angle. A reason for this might be the fact that these targets have surface that are highly uneven and where multi-scaterring effects are important. Grass 2 target showed very strange reaction to incident light at different angles. For these grass targets, there was almost no difference between circular and linear reflectivity.

Concrete target showed larger reflectivity than asphalt, which is reasonable considering the black color of asphalt. Correspondingly, depolarization ratio of concrete is more than that of asphalt. This is consequent with the fact that targets with higher reflectivity usually show more depolarization. Though linear depolarization ratio of concrete decreased slightly with incident angle from 15 ° to 45 °, the circular one increased with incident angle. This suggest that the depolarization ratio of both concrete and asphalt increased slightly with the incident angle.

Grass 2 target showed higher reflectivity than grass 1 (T4), and also more depolarization ratio of T5 than that of T4. this is consequent with previous observations. However, the depolarization ratios of grasses seemed to be independent to the inci-

dent angle. This might be because of the very uneven surface of the grass and of multi-scaterring effects.

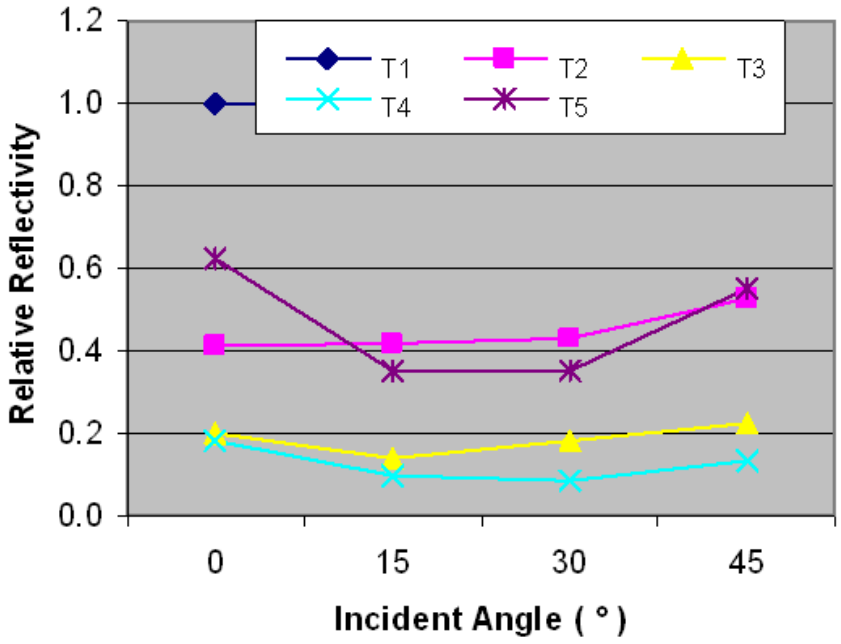

(a) δ_L

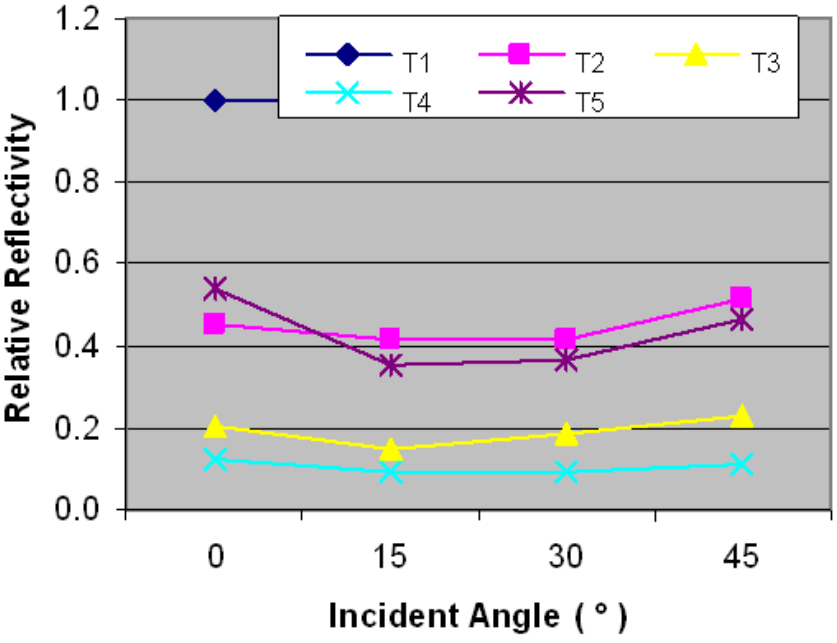

(b) δ_C

Figure 40: *Relative 40(a) linear reflectivities, and 40(b) circular reflectivity of construction and grass targets and their changes with incident angle*

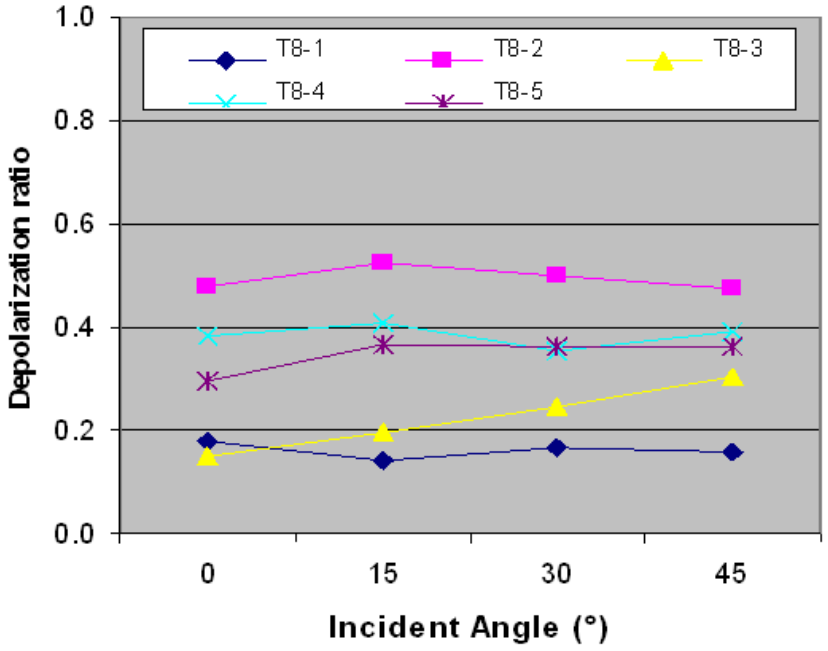

(a) δ_L

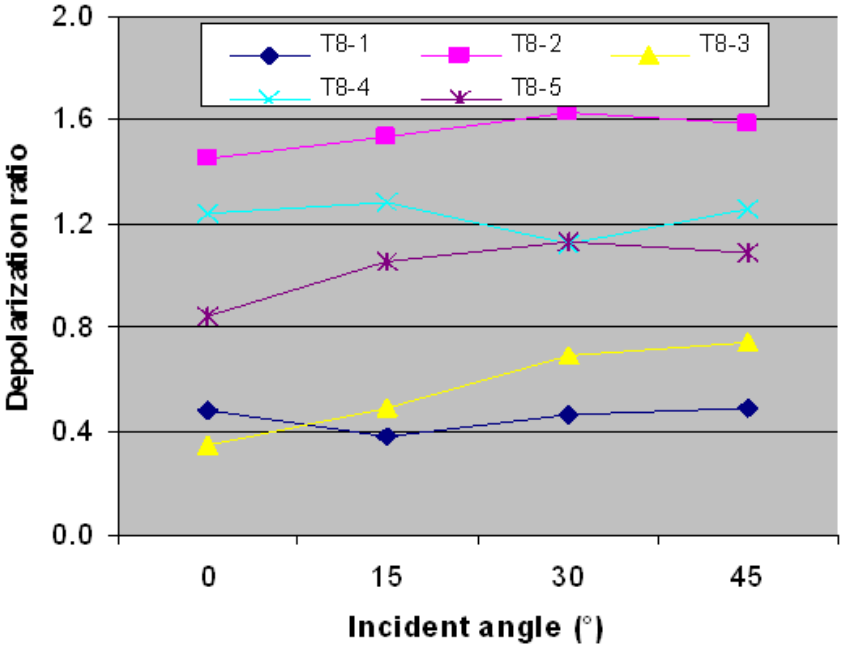

(b) δ_C

Figure 41: *Depolarization ratios of construction and grass targets and their changes with incident angle.*

5 Summary of the experimental results

Based on the analysis of all targets, the ones with light color and smooth surface showed higher reflectivity than the ones with dark color and rough surface. Circular polarization reflectivity is usually close to the linear reflectivity with the exception of some targets where the ratio was close to 2.0. It is also found that for most solid targets in same material category, targets with higher reflectivity usually showed more depolarization ratio than targets with lower reflectivity. Depolarization ratio increased with light incident angle, and circular depolarization ratio is usually $2 \sim 3$ times of the linear one for most targets, with a few exceptions. Each material category is summarized as follows:

1. **Panel 1 - Insulation targets.** Relative reflectivity of insulation targets decreased with the incident angle: the lighter the surface color and the smoother the surface, the more decline the reflectivity with the incident angle. Depolarization ratio increased with the incident angle, approximately linearly with reflectivity.

2. **Panel 2 - Wood targets.** Both reflectivity and depolarization ratios of wood targets increased with the incident angle, but not to the same extent as insulation targets. Still, the depolarization ratio of wood targets increased slightly with reflectivity.

3. **Panel 3 - Metallic targets.** Metallic targets with smooth surfaces and light colors showed much higher reflectivity than white Spectralon at incident angle of 0°. Then, it dropped sharply when incident angle increased to 15°, followed by a slight decrease when light incident angle further increased. In that case, the reflectivity was below the white Spectralon reflectivity. The depolarization ratio of metallic targets increased with the incident angle. However, it showed extremely high reflectivity but fairly low depolarization ratios. From this point of view, metallic targets are special objects as they do not follow the general rules that depolarization ratio increases with reflectivity. The depolarization ratios of metallic targets are pretty stable or slightly decreased when reflectivity increased.

4. **Panel 4 - Environmental targets.** Relative reflectivity of enviromental targets decreased from incident angle 0° to 15°, then decreased gradually with the incident angle. All metallic targets showed lower reflectivity than white Spectralon. Both crashed or curved environmental targets made of same materials usually showed little difference of their reflectivity, but varied in depolarization ratios. The crushed ones usually showed more depolarization than non-crushed

ones. However, the depolarization ratio of crushed bottles or cans seemed insensitive to the incident angle. They remained practically unchanged with an increase of the incident angle. This might be because of uneven surface of those targets and some multi-scattering effects. As similar to wood and metallic targets, the depolarization ratios of environmental targets seemed little related to the reflectivity of those targets.

5. **Panel 5 - Sand paper targets.** Like metals, relative reflectivity of sand paper targets decreased with the incident angle. However, the decrease is smoother than for the metals. The depolarization ratios of sand paper targets increased with the incident angle. Similar to insulation targets, depolarization ratio of sand papers showed approximately a linear increase with reflectivity.

6. **Panel 6 - Composite plastic types.** As for metallic targets, composite plastic targets were composed of very smooth surfaces. Indeed, one target (i.e. *nema phenolic*) showed very similar reflectivity property as metallic targets. Most targets on panel 6 showed a decrease of the relative reflectivity and an increase of the depolarization ratios with incident angle. Depolarization ratio showed a quasi linear increase with target reflectivity, except target 14 (i.e. *polycarbonate resin thermoplastic*) which showed low reflectivity but very high depolarization ratio.

7. **Sand targets.** Coarse sands always showed less reflectivity than fine sands, no matter if it is dry or wet. Reflectivity of dry sands increased while it decreased with the incident angle for wet sand. As for the depolarization ratio, fine sands always showed more depolarization ratio than coarse sands. This is in agreement with most other targets: the depolarization ratio increased with reflectivity. Depolarization ratios hardly changed with incident angle from 0° to 30°.

8. **Construction material and grass targets.** Concrete and asphalt were examined and there was no surprise that higher reflectivity from concrete and more depolarization ratio showed up. Incident angle seemed to have no influence on reflectivity of these targets, mainly due to the very uneven surface. Circular depolarization showed somewhat increase with the incident angle, but not very obvious from linear depolarization ratio. In general, incident angle showed noticeable influence on reflectivity and depolarization when targets are fairly smooth surface. Relative reflectivity usually decreased with the incident angle, except the targets of different wood and some environmental targets where their reflectivity increased with the angle. Depolarization ratio increased with incident angle of polarized light for most targets, when their surface was

fairly smooth. As to the relationship between reflectivity and depolarization ratio, for targets of the same material category, targets with higher reflectivity usually showed more depolarization ratio, with the exception of high reflective metallic targets, highly curved ones, and targets with very rough surfaces.

This page intentionally left blank.

6 Depolarization ratio comparison with lidar of $1.57\mu m$

Previous experimental results were based on field measurements using a lidar of wavelength of 532 nm.

Other field measurements of depolarization of solid targets were conducted using $1.57\mu m$ wavelength lidar in September 2008. In this case, subtargets on each panel were examined individually. For most targets, only two incident angles were measured. These measurements were mainly used to compare depolarization ratios of pollens. However, these experiments could be useful to compare the results for the same targets but with different wavelengths. Table 24 shows analysis results of depolarization ratios of targets from panel 1 to 6, and corresponding materials can be found in Tables 1 to 19. Figure 42 shows comparison of depolarization ratios of some targets using the 532 nm and $1.57\mu m$ lidars.

Table 24: *Depolarization ratio comparison of some targets*

Target #	Linear Depolarization ratio (δ_L)											
	Panel 1		Panel 2		Panel 3		Panel 4		Panel 5		Panel 6	
	0 °	15 °	0 °	15 °	0 °	15 °	0 °	15 °	0 °	15 °	0 °	15 °
4	0.48	0.48	0.21	0.38	0.01	0.07	0.07	0.46	0.43	0.45	0.04	0.08
5	0.36	0.47	0.25	0.33	0.02	0.04	0.08	0.21	0.47	0.36	0.41	0.34
6	0.57	0.57	0.32	0.36	0.08	0.18	0.47	0.45	0.47	0.48	0.39	0.73
7	0.74	0.73	0.26	0.42	0.03	0.16	0.40	0.46	0.09	0.08	0.09	0.10
8	0.39	0.40	0.36	0.40	0.01	0.05	0.50	0.51	0.45	0.46	0.56	0.69
9	0.31	0.28	0.35	0.45	0.05	0.22	0.40	0.37	0.16	0.18	0.37	0.45
10	0.37	0.53	0.44	0.47	0.01	0.05	0.20	0.14	0.22	0.17	0.28	0.53
11	0.09	0.23	0.39	0.53	0.02	0.07	0.23	0.14	0.43	0.41	0.34	0.52
12	0.81	0.50	0.24	0.35	0.04	0.08	0.48	0.19	0.41	0.42	0.40	0.37
13	0.05	0.14	0.23	0.25		0.04	0.06	0.09	0.02	0.06	0.05	0.09
14	0.44	0.42	0.33	0.18	0.02	0.10	0.10	0.09	0.08	0.31	0.39	0.34
15	0.66	0.52			0.14	0.15					0.08	0.16

Most target depolarization ratios are sensitive to the lidar wavelength. Depolarization ratios generated from light of the $1.5\mu m$ lidar are more than those from light of the 532 nm lidar. Exceptions of some environmental targets are: panel 4 with curved or very uneven surfaces (like cans and bottles), target 14 on panel 6 which is special (i.e. low reflectivity but very high depolarization ratio), and target 10 on panel 6.

Figure 42 also shows that depolarization ratios at incident angle 15 ° are usually higher than those at 0 °, no matter which wavelength was used. However, it is not the case for those targets with curved and uneven surfaces such as plastic bottles (panel 4), targets 14 and 15 on panel 1 and target 14 on panel 2. Figure 42(b) shows that the depolarization ratios of metallic targets from the two lidars with different wavelengths

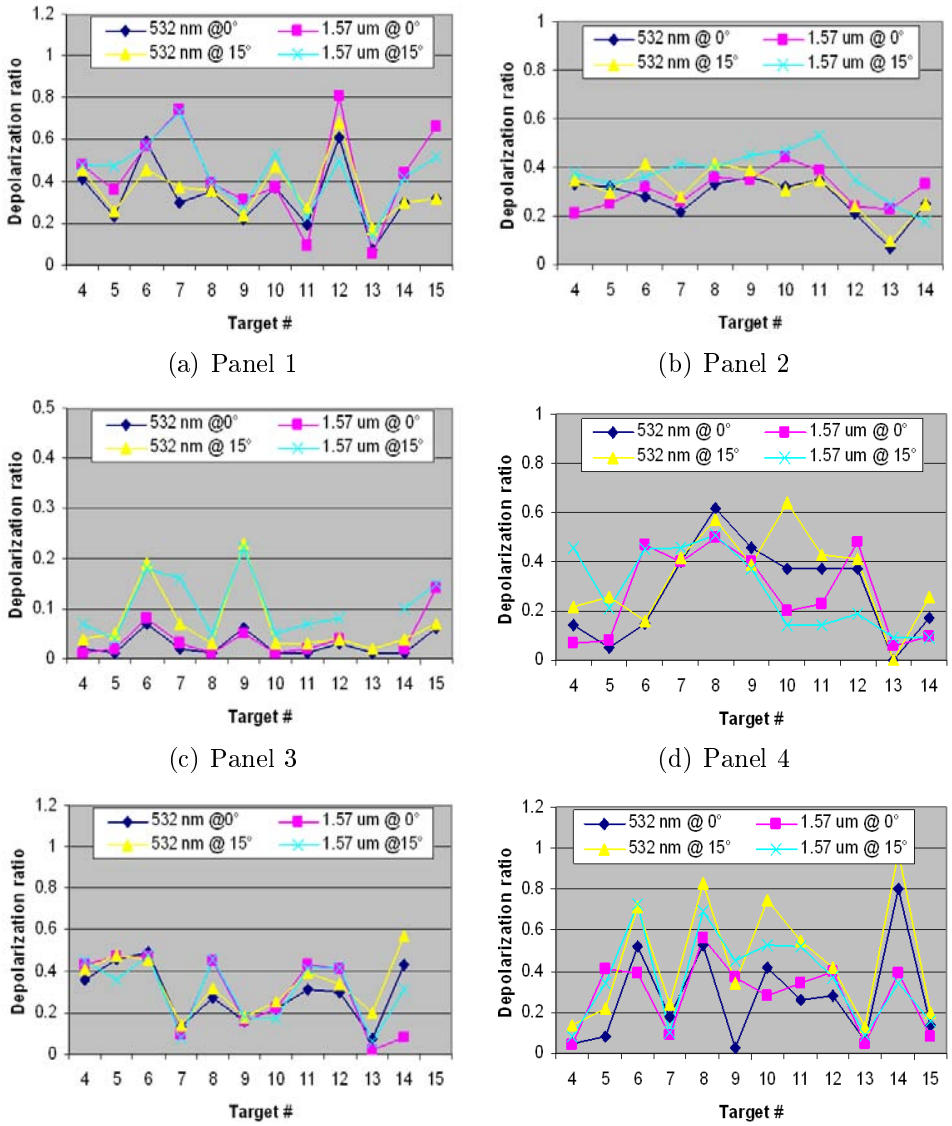

(a) Panel 1

(b) Panel 2

(c) Panel 3

(d) Panel 4

(e) Panel 5

(f) Panel 6

Figure 42: *Depolarization ratio comparison between 532 nm and 1.57μm lidars.*

are very close to each other. Sand papers are special materials too: their incident angles showed little influence on the depolarization ratios of those targets in the case of both wavelengths.

Environmental targets on panel 4 are complicated because they contained targets with smooth and very rough surfaces, and the results can be dramatically different if the light hits the target at different positions. Multi-scaterring may be greatly involved for targets with curved or very rough surfaces. This explains why the results from two wavelengths showed different trends for some targets, such as targets 10 and 11 that relatively high depolarization ratios were found with wavelength $532nm$, while relatively low depolarizations with $1.57\mu m$. Another example is target 7 and target 15 on panel 1, with fairly high values using the $1.57\mu m$ lidar.

Figure 42 also showed that depolarization ratios of wood and metallic targets are fairly stable. The depolarization ratios are located in the range $0.2 \sim 0.4$ for wood targets and around 0.05 for metallic targets when the incident angle was set at 0°. For other panel targets, relatively large range showed up particularly for targets on panel 6. Figure 42(f) shows that depolarization ratios of most targets on panel 6 are around 0.4 for those targets with lighter color.

This page intentionally left blank.

7 Conclusion and Future work

A field trial was carried out at DRDC Valcartier during 14-16 May 2008. The aim of this trial was to collect active polarization signatures of solid targets in order to discriminate them from their background. To do so, reflectivity and depolarization ratios of these solid targets have been measured with a dual image polarization lidar (consisting of a Q switch laser operating at 532 nm), a telescope and a gated intensified CCD camera from Andor Technology. Additionnaly, polarization signatures were also collected using a lidar operating at a wavelength of 1.57 μm. Different types of targets have been measured: construction materials and grass, textiles, woods, environmental targets, insulation materials, sands, composite plastics, and metals. The set-up was made of subtargets mounted onto a wooden board topped by a white and a black Spectralon. Multi-target boards were set up at four different angles (0°, 15°, 30°, 45°). Then, five polarized states (linear vertical, linear horizontal, circular left and circular right and *Retarders' Special*) were used. Since the depolarization results are based on the average counts, five images were acquired for each polarization state limiting the measuring noise. Therefore, twenty-five images were acquired at each angle and one hundred images were used for one set. Due to the small laser beam divergence, the multi-target board was then turned upside down so the second half of the targets could be measured.

Experimental results showed that reflectivity of most targets decreased with light incident angle with exception of wooden targets whose relative reflectivity increased with incident angle. The depolarization ratio usually increased with the incident angle, but sands and grasses are exceptionnal materials: their depolarization ratios changed little with the incident angle.

Targets with high reflectivity usually showed more depolarization too, with the exception of metallic targets which showed very high reflectivity at incident angle 0° but very low depolarization. Furthermore, they showed almost no correlation with the target reflectivity. The linear depolarization ratio linearly increased approximately with reflectivity if other properties of the targets are similar. Circular depolarization ratios are usually $2 \sim 3$ times of corresponding linear ones.

Linear depolarization ratios of targets measured from lidar operating at $1.57\mu m$ are usually higher than those from lidar operating at 532 nm. Nevertheless, this is not quite true for targets with curved or very rough surfaces and uneven color: they may show trends totally opposite to the above conclusions.

Wavelengths hardly affect the depolarization of most metallic targets; they are pretty similar for the influence of the incident angle on depolarization ratios of sand paper targets. Among all the panel targets, metals are the worst depolarizers, showing depolarization ratio less than 0.05. Other targets, as long as they are not of black

color, showed depolarization ratio around 0.4. Some of them may even reach a ratio up to 0.6, or even higher when they have high reflectivity.

For the measurements performed at different wavelengths, numerous ways to process the data have been used. The short wavelength lidar has already been described. For the measurement using wavelength of $1.57\mu m$ lidar, each subtarget was measured individually, thus fairly small divergent light beam was generated and the beam was fairly uniform. Very small part of each target was measured and used for the calculation of depolarization ratios. These two methods may not cause big changes in the results generated for targets with smooth surfaces, but it is very possible to produce large difference when targets surface are very rough or have uneven colors. Still, this has been noticed in the experimental results comparison using the two lidars.

The detection of target reflectivity greatly depends on the laser beam calibration. Since the calibration process was based on the average measurement of each pixel, and the aerosols in the air may not be always the same, the resulting calibration is not perfect for each measurement: sometimes relatively big errors may be induced. To avoid that the laser beam uniformity calibration scheme induced some calibration error, a small divergent laser beam measuring each target individually with the longer wavelength lidar was used.

The polarimetric signatures collected from solid targets will populate a reference library. Nonetheless, only two wavelengths have been used in the current research, which present some limitations about the conclusions that can be drawn. Future work will thus involved the collection of additional polarimetric signatures from new targets, at different wavelenghts, and including a wide range of backgrounds. Moreover, it would be worthwile to compare the experimental polarimetric signatures acquired against target models originating from a Modtran-P or through the use of a goniometer.

8 List of symbols/abbreviations/acronyms/initialisms

ARP	Applied Research Project
CCD	Charge-Coupled Device
DRDC	Defence Research and Development Canada
EO	Electro-Optic
G-ICCD	Gated Intensified Charge-Coupled Device
ICCD	Intensified Charge-Coupled Device
LIDAR	Light Detection And Ranging
LWIR	Long Wave InfraRed
MFOV	Medium Field Of View
Nd-YAG	Neodymium Doped Yttrium Aluminum Garnet
RDDC	Recherche et Développement pour la Défense Canada
WRT	With Respect To

This page intentionally left blank.

References

[1] Lavigne, D.A., Breton, M., Larochelle, V., and Simard, J-R. (2008), Evaluation of active and passive polarimetric electro-optic imagery for civilian and military targets discrimination, In *Proceedings of SPIE Defense and Security Symposium, Polarization: Measurement, Analysis, and Remote Sensing VII, Orlando (FL), 16-20 March.*

[2] Lavigne, D.A., Breton, M., Larochelle, V., and Simard, J-R. (2008), Enhanced military target discrimination using active and passive polarimetric imagery, In *IEEE International Geoscience & Remote Sensing Symposium (IGARSS) 2008, Boston (MA), 6-11 July.*

[3] Lavigne, D.A., Breton, M., Fournier, G., Pichette, M., and Rivet, V. (2008), Target enhancement using active and passive polarimetric images in the NIR and LIWR bands, In *9th Workshop on Infrared Remote Sensing Applications, Quebec (QC), 17-19 September.*

[4] Collett, E (2005), Field Guide to Polarization, SPIE field guides, SPIE Press.

[5] Chenault, D.B (2008), Polarization: Nomenclature and Background. Conference 6972 as part of SPIE's Defense and Security Symposium Polarization: Measurement, Analysis, and Remote Sensing VIII [PowerPoint presentation].

[6] Eliès, P., Le Jeune, B., Floc'h, M., Cariou, J., and Lotrian, J. (1997), Depolarization classification of metallic and dielectric targets, In *Proc. SPIE Vol. 3059*, pp. 174–182.

[7] Howe, J. D. and Buser, R.G. (2005), U.S. Army NVESD MWIR Polarization Research for Ground Targets, In Research, NATO and Organisation, Technology, (Eds.), *RTO-MP-SET-094 Emerging EO Phenomenology*, pp. 21–1 – 21–18.

[8] Lavigne, D.A., Breton, M., Fournier, G., Pichette, M., and Rivet, V. (2009), Development of performance metrics to characterize the degree of polarization of man-made objects using passive polarimetric images, In *Proceedings of SPIE Defense, Security and Sensing, Signal Processing, Sensor Fusion, and Target Recognition XVIII, Orlando (FL), 13-17 April.*

[9] Lavigne, D.A., Breton, M., Fournier, G., Pichette, M., and Rivet, V. (2009), A new passive polarimetric imaging system collecting polarization signatures in the visible and infrared bands, In *Proceedings of SPIE Defense, Security and Sensing, Infrared Systems; Design, Analysis, Modeling, and Tersting XX, Orlando (FL), 13-17 April.*

[10] Messelink, W.A.C.M., Schutte, K., Vossepoel, A.M., Cremer, F., Schavemaker, J.G.M., and Breejen, E. (2002), Feature-based detection of landmines in

infrared images, In *Proceedings of SPIE Vol. 4742: Det. and Rem. Techn. for Mine and Minelike Targets VII, Orlando Fl.*

[11] Scotland, R. M., Sassen, K., and Stone, R. (1971), Observations by lidar of linear depolarizations of hydrometeors, *J. Appl. Meteor.*, 10, 1011–1017.

[12] Sendur, I. K., Johnson, J. T., and Baertlein, B. A. (2001), Analysis of polarimetric IR phenomena for detection of surface mines, In Dubey, A. C., Harvey, J. F., Broach, J. T., and George, V., (Eds.), *Proc. SPIE Vol. 4394, p. 153-163, Detection and Remediation Technologies for Mines and Minelike Targets VI, Abinash C. Dubey; James F. Harvey; J. Thomas Broach; Vivian George; Eds.*, pp. 153–163.

[13] Breugnot, S. and Clémenceau, P. (2000), Modeling and performances of a polarization active imager at λ=806 nm, *Optical Engineering*, 39, 2681–2688.

[14] Clémenceau, P., Dogariu, A. C., and Stryjewski, J. S. (2000), Polarization active imaging, In Kamerman, G. W., Singh, U. N., Werner, C. H., and Molebny, V. V., (Eds.), *Proc. SPIE Vol. 4035, p. 401-409, Laser Radar Technology and Applications V, Gary W. Kamerman; Upendra N. Singh; Christian H. Werner; Vasyl V. Molebny; Eds.*, Vol. 4035 of *Presented at the Society of Photo-Optical Instrumentation Engineers (SPIE) Conference*, pp. 401–409.

[15] Cremer, F., de Jong, W., and Schutte, K. (2001), Infrared polarization measurements of surface and buried antipersonnel landmines, In Dubey, A. C., Harvey, J. F., Broach, J. T., and George, V., (Eds.), *Proc. SPIE Vol. 4394, p. 164-175, Detection and Remediation Technologies for Mines and Minelike Targets VI*, pp. 164–175.

[16] Harchanko, J.S. (2008), A comparison of MWIR and LWIR polarimetric imaging for surface swimmer detection, In *Proc. SPIE Vol. 6972*.

[17] Hori, M., Aoki, T., Tanikawa, T., Motoyoshi, H., Hachikubo, A., Sugiura, K., Yasunari, T.J., Eide, H., Storvold, R., Nakajima, Y., and Takahashi, F. (2006), In - situ measured spectral directional emissivity of snow and ice in the 8 - 14 μm atmospheric window, *Remote Sensing of Environment*, 100, 486 – 502.

[18] Koh, G. (1992), Laser Depolarization from targets in a Winter Environment, Technical Report U.S. Army Corps of Engineers: Cold Regions Research & Engineering Laboratory.

[19] Ben-Dor, B., Oppenheim, U. P., and Balfour, L. S. (1993), Polarization properties of targets and backgrounds in the infrared, In Oron, M., Shladov, I., and Weissman, Y., (Eds.), *Proc. SPIE Vol. 1971, p. 68-77, 8th Meeting on Optical Engineering in Israel: Optical Engineering and Remote Sensing, Moshe Oron; Itzhak Shladov; Yitzhak Weissman; Eds.*, Vol. 1971 of *Presented at the Society of Photo-Optical Instrumentation Engineers (SPIE) Conference*, pp. 68–77.

[20] Oppenheim, U. P. and Feiner, Y. (1995), Polarization of the reflectivity of paints and other rough surfaces in the infrared, *Applied Optics*, 34, 1664–1671.

[21] ScotlSassenand, K. (1991), The polarization lidar technique for cloud research: a review and current assessment, *Bull. Am. Meteor. Soc.*, 72, 1848–1866.

This page intentionally left blank.

DOCUMENT CONTROL DATA

1. ORIGINATOR (name and address)	2. SECURITY CLASSIFICATION (Including special warning terms if applicable)
Defence Research and Development Canada - Valcartier 2459 Pie-XI Blvd. North Quebec (Qc) G3J 1X5	Unclassified

3. TITLE (Its classification should be indicated by the appropriate abbreviation (S, C, R or U)

(U) Influence of solid target reflectivity and incident angle on depolarization ratio and reflected energy from polarized lights - Experimental results of the May 2008 field trial

4. AUTHORS (Last name, first name, middle initial. If military, show rank, e.g. Doe, Maj. John E.)

Lavigne, Daniel, A.

Breton, Mélanie

5. DATE OF PUBLICATION (month and year)	6a. NO. OF PAGES	6b .NO. OF REFERENCES
November 2009	88	20

7. DESCRIPTIVE NOTES (the category of the document, e.g. technical report, technical note or memorandum. Give the inclusive dates when a specific reporting period is covered.)

Technical Report

8. SPONSORING ACTIVITY (name and address)

9a. PROJECT OR GRANT NO. (Please specify whether project or grant)	9b. CONTRACT NO.
15dk03	

10a. ORIGINATOR'S DOCUMENT NUMBER	10b. OTHER DOCUMENT NOS
	N/A

11. DOCUMENT AVAILABILITY (any limitations on further dissemination of the document, other than those imposed by security classification)

- ☒ Unlimited distribution
- ☐ Restricted to contractors in approved countries (specify)
- ☐ Restricted to Canadian contractors (with need-to-know)
- ☐ Restricted to Government (with need-to-know)
- ☐ Restricted to Defense departments
- ☐ Others

12. DOCUMENT ANNOUNCEMENT (any limitation to the bibliographic announcement of this document. This will normally correspond to the Document Availability (11). However, where further distribution (beyond the audience specified in 11) is possible, a wider announcement audience may be selected.)

Unlimited

13. ABSTRACT (a brief and factual summary of the document. It may also appear elsewhere in the body of the document itself. It is highly desirable that the abstract of classified documents be unclassified. Each paragraph of the abstract shall begin with an indication of the security classification of the information in the paragraph (unless the document itself is unclassified) represented as (S), (C), (R), or (U). It is not necessary to include here abstracts in both official languages unless the text is bilingual).

Spectral sensors are commonly used to measure the intensity of optical radiation and to provide spectral information about the distribution of material components in a given scene, over a limited number of wave bands. By exploiting the polarization of light to measure information about the vector nature of the optical field across a scene, collected polarimetric images have the potential to provide additional information about the shape, shading, roughness, and surface features of targets of interest. The overall performance of target detection algorithms could thus be increased by exploiting these polarimetric signatures to discriminate man-made objects against different backgrounds.

In order to understand how the polarisation of light might help in the discrimination of solid targets from their background, a field trial was conducted at DRDC Valcartier between 14-16 May 2008. The approach consisted in evaluating the depolarization ratio of different solid targets using active polarization signatures at 532 nm. This technical report presents the set-up, the methodology and the type of targets measured during the trial. The targets used were segmented into eight groups: insulation, wood, metallic, environment, sand paper-type, industrial plastic-type, bottles and sand targets. Experimental results on the influence of solid target reflectivity and incident angle on depolarization ratio and reflected energy from polarized lights is also provided.

14. KEYWORDS, DESCRIPTORS or IDENTIFIERS (technically meaningful terms or short phrases that characterize a document and could be helpful in cataloguing the document. They should be selected so that no security classification is required. Identifiers, such as equipment model designation, trade name, military project code name, geographic location may also be included. If possible keywords should be selected from a published thesaurus, e.g. Thesaurus of Engineering and Scientific Terms (TEST) and that thesaurus-identified. If it is not possible to select indexing terms which are Unclassified, the classification of each should be indicated as with the title.)

Polarimetric imaging, polarization, polarized light, active imaging, lidar, solid target reflectivity, depolarization ratio, reflected energy, incident angle.

Defence R&D Canada

Canada's Leader in Defence
and National Security
Science and Technology

R & D pour la défense Canada

Chef de file au Canada en matière
de science et de technologie pour
la défense et la sécurité nationale

www.drdc-rddc.gc.ca